



저작자표시-비영리-변경금지 2.0 대한민국

이용자는 아래의 조건을 따르는 경우에 한하여 자유롭게

- 이 저작물을 복제, 배포, 전송, 전시, 공연 및 방송할 수 있습니다.

다음과 같은 조건을 따라야 합니다:



저작자표시. 귀하는 원저작자를 표시하여야 합니다.



비영리. 귀하는 이 저작물을 영리 목적으로 이용할 수 없습니다.



변경금지. 귀하는 이 저작물을 개작, 변형 또는 가공할 수 없습니다.

- 귀하는, 이 저작물의 재이용이나 배포의 경우, 이 저작물에 적용된 이용허락조건을 명확하게 나타내어야 합니다.
- 저작권자로부터 별도의 허가를 받으면 이러한 조건들은 적용되지 않습니다.

저작권법에 따른 이용자의 권리는 위의 내용에 의하여 영향을 받지 않습니다.

이것은 [이용허락규약\(Legal Code\)](#)을 이해하기 쉽게 요약한 것입니다.

[Disclaimer](#)

Master's Thesis
석사 학위논문

**Influence of electrolyte constitution on metal dissolution
and surface free energy correlation
for lithium ion battery cathode**

Sung-Mo Choi(최 성 모 崔 成 模)

Department of Energy Systems Engineering
에너지시스템공학 전공

DGIST

2015

Master's Thesis
석사 학위논문

**Influence of electrolyte constitution on metal dissolution
and surface free energy correlation
for lithium ion battery cathode**

Sung-Mo Choi(최 성 모 崔 成 模)

Department of Energy Systems Engineering

에너지시스템공학 전공

DGIST

2015

Influence of electrolyte constitution on metal dissolution and surface free energy correlation for lithium ion battery cathode

Advisor : Professor Hochun Lee

Co-advisor : Doctor Jae-Hyun Kim

by

Sung-Mo Choi

Department of Energy Systems Engineering
DGIST

A thesis submitted to the faculty of DGIST in partial fulfillment of the requirements for the degree of Master of Science in the Department of Energy Systems Engineering. The study was conducted in accordance with Code of Research Ethics¹

12.05. 2014

Approved by

Professor Hochun Lee _____ (Signature)
(Advisor)

Doctor Jae-Hyun Kim _____ (Signature)
(Co-Advisor)

¹ Declaration of Ethical Conduct in Research: I, as a graduate student of DGIST, hereby declare that I have not committed any acts that may damage the credibility of my research. These include, but are not limited to: falsification, thesis written by someone else, distortion of research findings or plagiarism. I affirm that my thesis contains honest conclusions based on my own careful research under the guidance of my thesis advisor.

**Influence of the electrolyte constitution on the metal dis-
solution and surface free energy correlation
for lithium ion battery cathode**

Sung-Mo Choi

Accepted in partial fulfillment of the requirements for the degree of
Master of Science

12.05. 2014

Head of Committee _____(인)

Prof. Hochun Lee

Committee Member _____(인)

Dr. Jae-Hyun Kim

Committee Member _____(인)

Prof. Seung-Tae Hong

MS/ES
201324012

최 성 모. Sung-Mo Choi. Influence of the electrolyte constitution on the metal dissolution and surface free energy correlation for lithium ion battery cathode. Department of Energy Systems Engineering. 2015. 62p. Advisors Prof. Hochun Lee, Co-Advisor Dr. Jae-hyun Kim.

ABSTRACT

The quantitative analysis of dissolved metal ions has been dependent on the spectroscopic techniques such as the inductive coupled plasma (ICP). This conventional method takes at least several days. Also it is easily fail to provide any information on the cathode surface properties. Therefore we examine that the SFE of cathode materials is closely related to their metal dissolution behavior. We confirm that the metal dissolution is determined dominantly by the total and acid SFE of the $\text{LiNi}_{0.6}\text{Co}_{0.2}\text{Mn}_{0.2}\text{O}_2$ cathode surface.

The cell degradation of cathode material which is LiMn_2O_4 (LMO) for Lithium ion battery (LIB) is severe problem due to manganese dissolution. Because Mn dissolution is electrode/electrolyte interfacial phenomenon, it is important to analyze the electrolyte constitution. However, more detailed research about the relationship between the electrolyte property and Mn-dissolution has not been carried out so far. Therefore, to investigate the effects of electrolyte on the Mn dissolution, the various change in electrolyte compositions were employed for Mn dissolution experiments. We conclude that increasing EC content, storage duration and elevated temperature promote to Mn-dissolution. We analyze the unreacted core model for spherical particles with fixed size such as the penetration of soluble Mn^{2+} ions through electrolyte, chemical reaction and diffusion controlled through the product layer. When increasing EC content, it diminish the activation energy of dissolution on electrode/electrolyte interface.

We focused on the better understanding of the adsorption behavior of liquid electrolyte on electrodes. The main purpose is to determine the γ^+ , γ^- and γ^d values of battery electrolyte such as propylene carbonate (PC) and dimethyl sulfoxide (DMSO) by using wafer, polystyrene and aluminium. These results will provide valuable guidance for calculate the surface free energy of electrolyte. Eventually, we can get Lewis acid component or the electron acceptor (γ^+) and Lewis base component or the electron donor (γ^-) component of liquid electrolyte based on SFE of solid surface tension such as wafer, polystyrene, aluminum oxide.

Keywords: LiMn_2O_4 , $\text{LiNi}_{0.6}\text{Co}_{0.2}\text{Mn}_{0.2}\text{O}_2$, electrolyte, Surface free energy, metal dissolution, Propylene carbonate, dimethyl sulfoxide

Contents

Abstract	i
List of contents	ii
List of tables	iv
List of figures	v

I . Surface free energy measurement to assess metal dissolution behavior of layered oxide

LiNi_{0.6}Co_{0.2}Mn_{0.2}O₂

1 Introduction	1
1.1 Overview	1
1.2 Theory of surface free energy calculation	3
1.3 Capillary rising method for porous materials	9
1.4 Examples of surface free energy usages to analyze the Li ion batteries	11
2 Experimental	12
2.1 Adsorption method	12
2.2 Preparation of NCM electrode	15
2.3 Metal dissolution	16
3 Results and discussion	17
3.1 Metal dissolution and SFE of Al coated LiNi _{0.6} Co _{0.2} Mn _{0.2} O ₂	17
3.2 Analysis of the morphology of Al coated LiNi _{0.6} Co _{0.2} Mn _{0.2} O ₂	20
3.3 Connection between SFE and metal dissolution of Al coated LiNi _{0.6} Co _{0.2} Mn _{0.2} O ₂	21
4 Conclusions	25

II . Influence of the electrolyte constitution on the dissolution kinetics of manganese from LiMn₂O₄ cathode for lithium ion battery

1 Introduction	27
2 Experimental	32
3 Results and discussion	34
3.1 Effects of EC content, reaction temperature and storage time on Mn dissolution	34
3.2 Kinetics of Mn dissolution	36

3.3 The penetration of soluble Mn^{2+} ions through electrolyte controlled process	36
3.4 Chemical reaction controlled process	37
3.5 Diffusion controlled through the product layer	39
3.6 Activation energy determination.....	42
3.7 Effect of solvation energy and HF	44
4 Conclusions.....	47

III. Analysis of surface free energy in battery electrolytes.

1 Introduction	48
2 Experimental	50
3 Results and discussion	52
3.1 Characterization of reference materials.....	52
3.2 The surface free energy calculation of propylene carbonate	55
4 Conclusions.....	58

List of tables

Table 1. Critical surface tensions of polymeric solids

Table 2. N/Metal and S/Metal ratios measured by XPS after adsorption of NH₃ or CO₂ at 80°C on LiCo_{1-x}Al_xO₂ Samples (0 ≤ x ≤ 0.50), compared with various oxides in the same experimental conditions

Table. 3. Correlations of SFEs and Ni dissolution of LiNi_{0.6}Co_{0.2}Mn_{0.2}O₂ by using correlation coefficient and P-value

Table. 4. Correlations of SFEs and Co dissolution of LiNi_{0.6}Co_{0.2}Mn_{0.2}O₂ by using correlation coefficient and P-value

Table. 5. Correlations of SFEs and Mn dissolution of LiNi_{0.6}Co_{0.2}Mn_{0.2}O₂ by using correlation coefficient and P-value

Table 6. SFE properties of probe liquids

Table.7. Surface free energy and its dispersive, polar, Lewis acid and base components for Al₂O₃ with the vOCG equation

Table.8. Surface free energy and its dispersive, polar, Lewis acid and base components for PS with the vOCG equation.

Table.9. Surface free energy and its dispersive, polar, Lewis acid and base components

for wafer with the vOCG equation.

Table. 10. Surface free energy of PC by using 2 probe solids (PS, Wafer).

Table. 11. Surface free energy of PC by using 2 probe solids (Wafer, Al₂O₃).

Table 12. Surface free energy of PC by using 2 probe solids (PS, Al₂O₃)

**Table 13. Surface free energy of dimethyl sulfoxide(DMSO) by using 2 probe solids
(PTFE, Wafer)**

List of figures

Fig. 1. A very simple Fowkes' model of interface.

Fig. 2. Schematic experimental setup for contact angle measurements at powders.

Fig. 3. Fiber chamber.

Fig. 4. Formamide adsorption mass change by time of $\text{LiNi}_{0.6}\text{Co}_{0.2}\text{Mn}_{0.2}\text{O}_2$ powder.

Fig. 5. Adsorbed mass of probe liquids to filter.

Figure. 6. Contact angle from adsorption method by using (a) water (b) diiodomethane (c) formamide.

Figure. 7. Surface free energy components.

Figure. 8. Mn dissolution of 1M LiPF_6 EC/EMC(3:7) after high temperature (60°C) storage for 14days.

Fig. 9. SEM images of $\text{LiNi}_{0.6}\text{Co}_{0.2}\text{Mn}_{0.2}\text{O}_2$ powders by increasing particle size (a) $4\ \mu\text{m}$, (b) $10\ \mu\text{m}$, (c) $10\ \mu\text{m}$, and (d) $15\ \mu\text{m}$.

Fig. 10. Correlations of SFEs and Ni dissolution of $\text{LiNi}_{0.6}\text{Co}_{0.2}\text{Mn}_{0.2}\text{O}_2$.

Fig. 11. Correlations of SFEs and Co dissolution of $\text{LiNi}_{0.6}\text{Co}_{0.2}\text{Mn}_{0.2}\text{O}_2$.

Fig. 12. Correlations of SFEs and Mn dissolution of $\text{LiNi}_{0.6}\text{Co}_{0.2}\text{Mn}_{0.2}\text{O}_2$.

Fig. 13. Schematic illustration of $\text{LiNi}_{0.6}\text{Co}_{0.2}\text{Mn}_{0.2}\text{O}_2$ dissolution mechanisms

Fig. 14. Schematic illustration of Mn dissolution mechanisms.

Fig. 15. Schematic diagram controlled by diffusion reaction LiMn_2O_4 in electrolyte for EC/EMC ratio changes (EC=10, 30, 90%).

Fig. 16. Fig. 15. Schematic diagram controlled by chemical reaction LiMn_2O_4 in electrolyte for EC/EMC ratio changes (EC=10, 30, 90%).

Fig. 17. Schematic diagram controlled by diffusion through the product layer LiMn_2O_4 in electrolyte for EC/EMC ratio changes (EC=10, 30, 90%).

Fig. 18. Procedure of Mn dissolution experiment to investigate the content of water and HF, and the concentration of dissolved Mn^{2+} ion in the electrolyte at various temperature storage (35°C, 45°C, 55°C and 65°C.).

Fig. 19. Mn dissolution of 1 M LiPF_6 EC/EMC (1/9, 3/7, 9/1 by volume) at various temperature (35°C, 45°C, 55°C and 65°C) storage for 2, 9, 19, 29, 36, 46 and 56 days

Fig. 20. The penetration of soluble Mn^{2+} ions through electrolyte mechanisms are plotted for various temperatures and EC/EMC ratio changes (EC=10, 30, 90%)

Fig. 21. Chemical reaction mechanisms are plotted for various temperatures and EC/EMC ratio changes (EC=10, 30, 90%)

Fig. 22. Diffusion through the product layer mechanisms are plotted for various tem-

peratures and EC/EMC ratio changes (EC=10, 30, 90%).

Fig. 23. Arrhenius plot for the dissolution of manganese for EC/EMC ratio (1:9).

Fig. 24. Arrhenius plot for the dissolution of manganese for EC/EMC ratio (3:7).

Fig. 25. Arrhenius plot for the dissolution of manganese for EC/EMC ratio (9:1).

Fig. 26. Mn dissolution of 1M LiClO₄ X/EMC (1:1mol, X=EMC, EC, 1G, TMP or DMSO) for various HF contents.

Fig. 27. Mn dissolution of 1M LiTFSI X/EMC (1:1mol, X=EMC, EC, 1G, TMP or DMSO) for various HF contents.

Fig. 28. Mn dissolution of 1M LiPF₆ X/EMC (1:1mol, X=EMC, EC, 1G, TMP or DMSO).

Fig. 29. Contact angle with reference liquids on Al₂O₃.

Fig. 30. Contact angle with reference liquids on PS.

Fig. 31. Contact angle with reference liquids on wafer.

Fig. 32. Contact angle with reference liquids on propylene carbonate.

Fig. 33. Contact angle with reference liquids on propylene carbonate

Fig. 34. Contact angle with reference liquids on dimethyl sulfoxide(DMSO)

I . Surface Free Energy Measurement to Assess Metal Dissolution Behavior of Layered Oxide $\text{LiNi}_{0.6}\text{Co}_{0.2}\text{Mn}_{0.2}\text{O}_2$

1.1. Introduction

1.1 Overview

NCM is one of promising candidates for electrical vehicles for high power with long cycle life. But degradation of cycle life is one of serious problem of $\text{LiNi}_{0.6}\text{Co}_{0.2}\text{Mn}_{0.2}\text{O}_2$. Main cause of cycle life degradation is metal dissolution of cathode. So this study mainly focused on to characterize the surface free energies (SFEs) of $\text{LiNi}_{0.6}\text{Co}_{0.2}\text{Mn}_{0.2}\text{O}_2$ for LIBs to predict metal dissolution.

Contact angles were measured to calculate SFEs of cathodes. They were measured by the liquid adsorption method for various powder samples. The contact angles of $\text{LiNi}_{0.6}\text{Co}_{0.2}\text{Mn}_{0.2}\text{O}_2$ powders were calculated from mass changes of porous cathode by adsorbing probe liquids by time. But cathode electrodes had many noises due to the mixture of cathode powder, conductive carbon and binder. Therefore, $\text{LiNi}_{0.6}\text{Co}_{0.2}\text{Mn}_{0.2}\text{O}_2$ powders should be used to examine the real characteristic cathode powders. Metal dissolution of $\text{LiNi}_{0.6}\text{Co}_{0.2}\text{Mn}_{0.2}\text{O}_2$ were done by atomic adsorption spectroscopy (AAS) (Shimadzu AA7000) to confirm the correlation with SFEs.

According to vOCG the SFE of liquid surface tension can be expressed as the sum of two components, $\gamma = \gamma^{\text{LW}} + \gamma^{\text{AB}}$. In this equation, γ^{AB} is the component resulting from Lewis acid-base intermolecular interactions. The γ^{AB} component can be expressed to the equation $\gamma^{\text{AB}} = 2(\gamma^+ \gamma^-)^{1/2}$, where γ^+ and γ^- are the nonadditive parts of the liquid surface tension.

The total surface free energy of a liquid is easily obtained by using ring method. And then, a

set of three solid is required to calculate the SFE components for the liquid, by means of the vOCG equations [Eq 13].

1.2 Theory of surface free energy calculation by contact angle measurements

The investigation of interaction between liquid and solid by contact angle measurement has begun from early 18th century by Thomas Young[1]. Thanks to these studies, the calculation method of SFE was suggested by D. K. OWENS in 1969[2]. He analyzed surface energy of solids and resolved the surface energy into dispersion and dipole-hydrogen bonding forces by based on measuring contact angles by using water and methylene iodide. Especially, measured surface energies were well matched with Zisman's γ_c (Critical Surface Tension: Total surface energy) [3] and Fowkes' γ_d (Dispersion Force)[4].

Polymeric Solid	γ_c
Polymethacrylic ester of Φ -octanol ^a	10.6
Polyhexafluoropropylene	16.2
Polytetrafluoroethylene	18.5
Polytrifluoroethylene	22
Polyvinylidene fluoride	25
Polyvinyl fluoride	28
Polyethylene	31
Polytrifluorochloroethylene	31
Polystyrene	33
Polyvinyl alcohol	37
Polymethyl methacrylate	39
Polyvinyl chloride	40
Polyvinylidene chloride	40
Polyethylene terephthalate	43
Polyhexamethylene adipamide	46

Table 1. Critical surface tensions of polymeric solids [3]

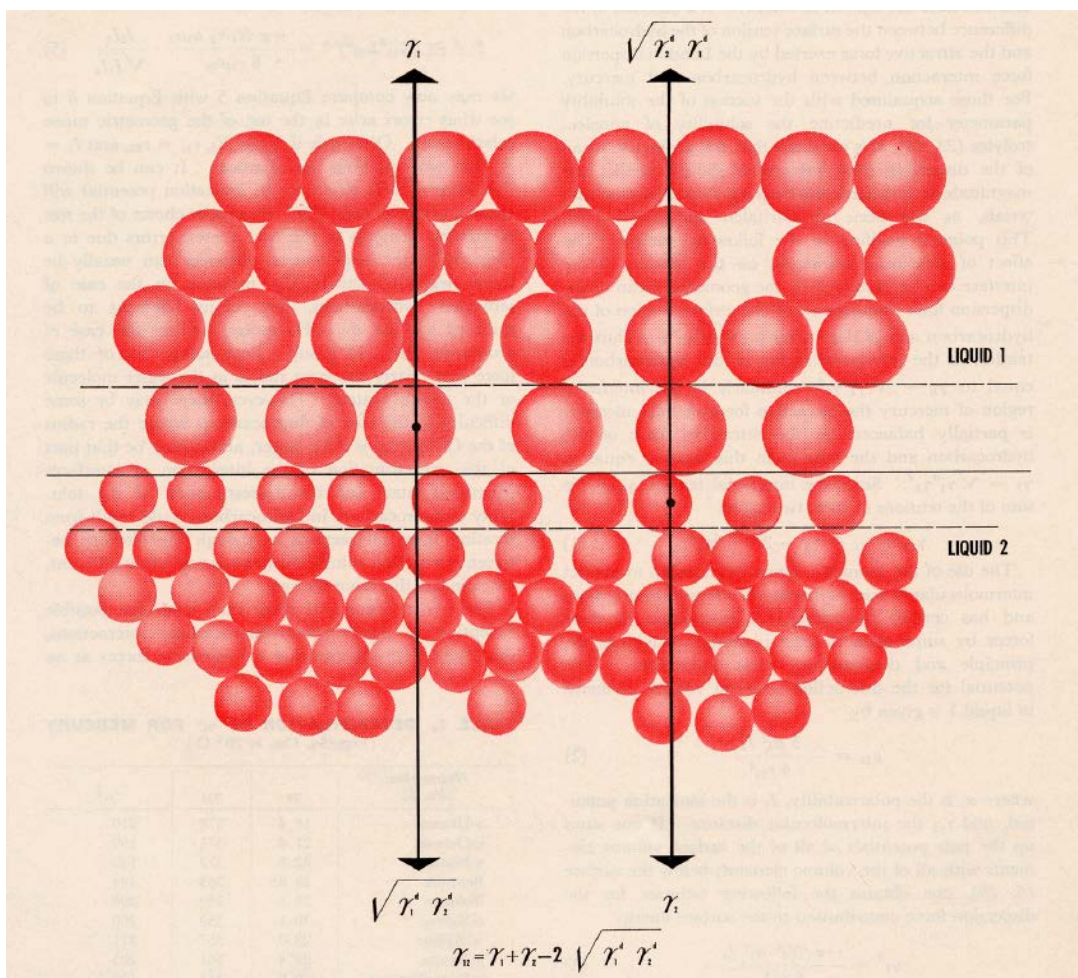


Fig. 1. A very simple Fowkes' model of interface [4]

At the interface between mercury and a saturated hydrocarbon the molecules in the two “interfacial region” are subject to the resultant force field made up of components arising from bulk attractive forces in each phase, and the London dispersion forces operating across the interface itself [4].

C.J. van Oss, M.K. Chaudhury and R.J. Good (vOCG) divided polarity of monopolar surface into acid and base part of SFE in 1987 [5]. Bronislaw Jańczuk summarized the components of the surface tension of some liquids from interfacial liquid-liquid tension measurements in 1993 [6]. Sum up the study of Bronislaw Jańczuk, the liquid surface tension or solid

SFE can be expressed as the sum of the parts of different kind of intermolecular interactions [7].

$$\gamma = \gamma^d + \gamma^i + \gamma^p + \gamma^h + \gamma^\pi + \gamma^{ad} + \gamma^e \quad (\text{Eq. 1})$$

where γ is the surface tension of a liquid or the solid SFE, and index d refers to dispersion, I refer to induced dipole-dipole, p to dipole-dipole, h to hydrogen bonding, π to π bonding, e to electrostatic, and ad to acceptor-donor interactions. Practically it can be written

$$\gamma = \gamma^d + \gamma^n \quad (\text{Eq. 2})$$

where γ^n is the nondispersion component of SFE of a liquid or solid surface tension. This component is sum of all parts of the surface tension resulting from the nondispersion intermolecular interactions present in a given phase.

The interfacial free energy of solid-liquid or liquid-liquid as a function of the geometric mean of dispersion and nondispersion intermolecular interaction [2, 7-9] can be expressed

$$\gamma_{12} = \gamma_1 + \gamma_2 - 2(\gamma_1^d \gamma_2^d)^{1/2} - 2(\gamma_1^n \gamma_2^n)^{1/2} \quad (\text{Eq. 3})$$

where 1 and 2 refer to two immiscible phases in contact with their own vapor, and the index 12 refers to two phases being in contact with each other after equilibration. The component of the liquid surface tension (γ_1^d value, γ_2^d and γ_2^n) can be calculated from Eq2 and 3 on the

basis of interfacial tension (γ_{12}) measurements. If the liquid 1 is hydrocarbon Eq. 3 can be rewritten.

$$\gamma_2^d = (\gamma_1 + \gamma_2 - \gamma_{12})^2 / 4\gamma_1 \quad (\text{Eq.4})$$

The dispersion and nondispersion components can be also be calculated on the basis of the Young's equation [1,2,7-9].

$$\gamma_L \cos \theta_L = -\gamma_L + 2(\gamma_L^d \gamma_S^d)^{1/2} + 2(\gamma_L^n \gamma_S^n)^{1/2} \quad (\text{Eq. 5})$$

L and S refer to liquid and solid, respectively. If γ_S^d and γ_S^n are known for a given liquid on the surface of two different solids, γ_L^d and γ_L^n can be easily calculated by Eq. 5. In the case when SFE of solid results only from dispersion intermolecular interactions Eq. 5 can be resolved into the form

$$\gamma_L^d = \gamma_L^2 (\cos \theta_L + 1)^2 / 4\gamma_S \quad (\text{Eq. 6})$$

vOCG [5, 10, 11] suggest that from Eq. 4 there can be obtained the components of the surface tension resulting from Lifshitz-van der Waals intermolecular interactions, which constitute the equation

$$\gamma^{LW} = \gamma^d + \gamma^i + \gamma^p \quad (\text{Eq. 1-7}).$$

According to vOCG [11] the SFE of solid or liquid surface tension can be expressed as the sum of two components,

$$\gamma = \gamma^{LW} + \gamma^{AB} \quad (\text{Eq.8})$$

where γ^{AB} is the component resulting from Lewis acid-base intermolecular interaction.

The γ^{AB} component can be expressed to the equation

$$\gamma^{AB} = 2(\gamma^+\gamma^-)^{1/2} \quad (\text{Eq. 9})$$

where γ^+ and γ^- are the nonadditive parts of the liquid surface tension or solid SFE resulting from electron-accepter and electron-donor interactions, respectively.

Combining Eq. 9 into 8, we have

$$\gamma = \gamma^{LW} + 2(\gamma^+\gamma^-)^{1/2} \quad (\text{Eq. 10})$$

Considering Eq. 10, vOCG [5, 10, 11] derived the equation describing the work of adhesion of phase 1 to phase 2. In the case of two liquids that are in contact this equation assume the form

$$\gamma_1 + \gamma_2 \sim \gamma_{12} = 2(\gamma_1^{LW}\gamma_2^{LW})^{1/2} + 2(\gamma^+\gamma^-)^{1/2} + 2(\gamma^-\gamma^+)^{1/2} \quad (\text{Eq. 11})$$

In the case when $\gamma_L = \gamma_1$ Eq. 11 can be rewritten in the form of

$$\gamma_2^{LW} = (\gamma_1 + \gamma_2 - \gamma_{12})^2 / 4\gamma_1 \quad (\text{Eq. 12})$$

According to vOCG [5, 10, 11], exists between the contact angle and components of solid SFE and liquid surface tension can be expressed

$$\gamma_L(\cos\theta + 1) = 2(\gamma_S^{LW}\gamma_{L,i}^{LW})^{0.5} + 2(\gamma_S^+\gamma_{L,i}^-)^{0.5} + 2(\gamma_S^-\gamma_{L,i}^+)^{0.5} \quad (\text{Eq. 13})$$

We used Eq. 13 with three different probe liquids to calculate SFEs of cathode materials for Li-ion batteries.[12]

1.3 Capillary Rising Method for Porous Materials

Contact angles of porous powders can be measured by capillary rising method. According to Washburn, we can calculate the contact angle of porous powder by measuring adsorbed liquid height by times.

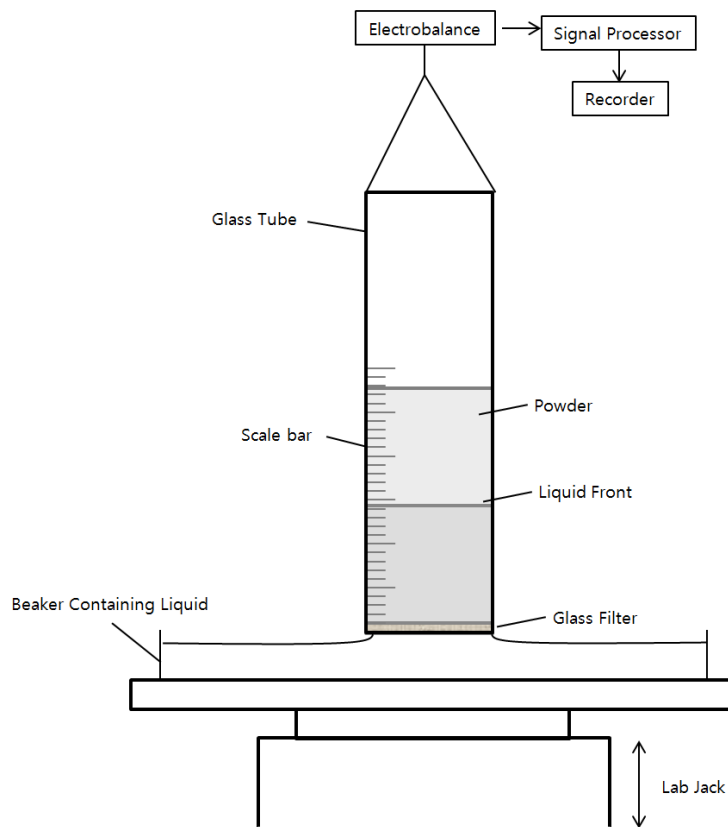


Fig. 2. Schematic experimental setup for contact angle measurements at powders[9]

Relations of capillary rising can be described by Washburn equation[13]

$$\frac{dh}{dt} = \frac{r^2}{8\eta h} \left(\frac{2\gamma_{lv}\cos\theta}{r} - \Delta\rho gh \right) \quad (\text{Eq. 14})$$

where h is the height of liquid penetration at time t , r is the radius of capillary. γ_{lv} Is the liquid to vapor surface tension, θ is the contact angle, $\Delta\rho$ is the difference in density between the liquid and the gas phase, and η is the viscosity. Washburn equation can be measured by detection of m^2/t and can be simplified by measuring capillary constant. Capillary constant can be obtained by measuring m^2/t with totally wetting liquid which is n-hexane.

$$\cos\theta = \frac{m^2}{t} \times \frac{\eta}{\rho^2 \sigma_L c} \quad (\text{Eq. 15})$$

$$c = \frac{1}{2} \pi^2 r^5 n_k^2 \quad (\text{Eq. 16})$$

where r is radius of the micro capillaries between powder particles, n_k is the number of powder particles. Capillary rising method cannot be used for above 90° : no liquid can penetrate to the powder above 90° [9, 13-15].

1.4 Examples of Surface Free Energy Usages to analyze the characteristics of Li-ion

Batteries

Surface polarity studies of alumina coated LiCoO₂ through measuring adsorbed CO₂ or NH₃ gaseous particles on the surface by XPS measurements were reported[16, 17].

sample	N/metal	S/metal
γ -Al ₂ O ₃	0.006	0.025
SnO ₂	0.051	0.023
TiO ₂ anatase	0.063	0.08
LiCoO ₂	0.06	0.75
LiCo _{0.75} Al _{0.25} O ₂	0.07	0.64
LiCo _{0.50} Al _{0.50} O ₂	0.06	0.36

Table 2. N/Metal and S/Metal ratios measured by XPS after adsorption of NH₃ or CO₂ at 80°C on LiCo_{1-x}Al_xO₂ Samples (0 ≤ x ≤ 0.50), compared with various oxides in the same experimental conditions [16]

Adsorbed CO₂ or NH₃ were decreased with increasing alumina ratio of cathode material:

Alumina lower the basicity of cathode material as it shown in table 1. But this method only predicts polarity of cathode material indirect way.

Surface polarity was also determined by using carbon dioxide adsorption micro calorimetry measurement: Carbon dioxide is acidic which expected to adsorbed more strongly on basic sites. CO₂ adsorption microcalorimetry measurements were carried out to determine the number, strength and strength distribution of the surface basic sites of the various cathode materials[18]. But it is also an indirect measurement.

2. Experimental

2.1 Adsorption Method

The adsorption method (capillary rise technique) was used to measure the contact angles of the cathode powders for the Li-ion batteries. Tensiometer K100 (Krüss, Hamburg, Germany) was used for contact angle measurement of cathode powders filled in SH0620 fiber chambers as showed in the Fig. 3.



Fig. 3. Fiber chamber SH0620 (Krüss, Hamburg, Germany)

All powder samples were also stored in a 110°C vacuum furnace for over one day before measurement to dehydrate. The properties of the cathode powders were changed according to the time exposed to air due to the humidity. Therefore the contact angles were measured

within one hour. Capillary constant must be measured to determine the contact angles of porous materials such as cathode powder for Li-ion batteries. The n-hexane was used to measure capillary constant which has only dispersity part, not any of polar part. So the capillary constant was calculated by using Washburn's equation due to the fact that the contact angle should be zero. So the $\cos\theta$ was equal to one. The other terms are constant so, we can calculate the capillary constant.

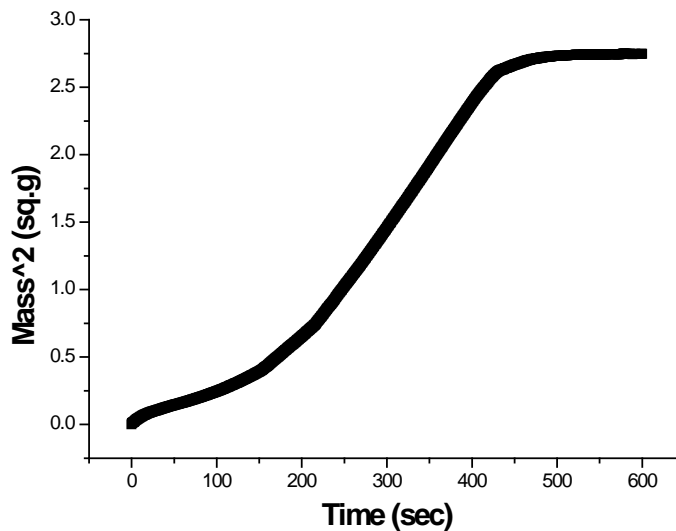


Fig. 4. Formamide adsorption mass change by time of $\text{LiNi}_{0.6}\text{Co}_{0.2}\text{Mn}_{0.2}\text{O}_2$ powder

After that, by measuring mass changes by the adsorption of known probe liquids by time, the contact angles of powder cathode by each probe liquids were calculated by using Washburn equation (Eq. 3). The mass square changes by time were chosen of its maximum gradient after the filter noises. Fig. 4 showed mass changes by adsorbing probe liquid time of

LiNi_{0.6}Co_{0.2}Mn_{0.2}O₂ powder.

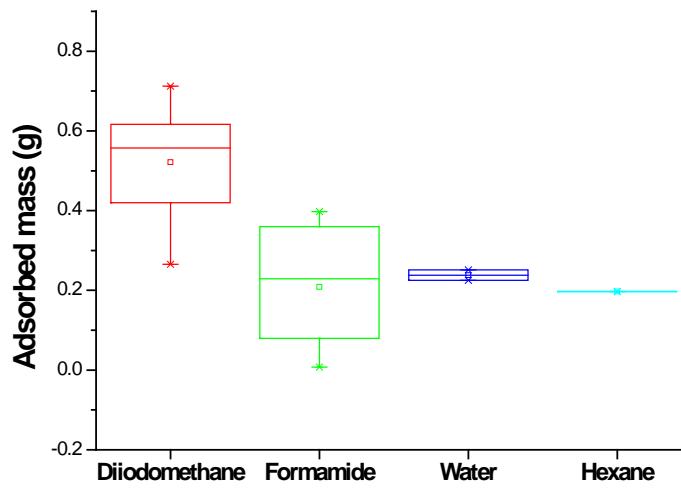


Fig. 5. Adsorbed mass of probe liquids to filter

Fig. 5 showed the adsorbed mass of probe liquids to filter. Diiodomethane adsorbed more and rapidly to the powder cathode than other probe liquids. So diiodomethane needed more cautious to loading the powder. To calculate SFEs of porous material the van Oss-Chaudhury-Good (vOCG) equation was used.

$$\cos \theta = \frac{m^2}{t} \times \frac{\eta}{\rho^2 \sigma_L c}$$

Eq. 17. Washburn's equation[13]

2.2 Preparation of NCM electrode

Cathode slurry was prepared by combining NCM powder (L&F Co., Korea) as active material, Super-p as conductive carbon and PVdF (KF 1300, Kureha) as binder. NMP was used as solvent to adjust the viscosity of the slurry. The four ball-milled slurries were uniformly coated onto Al foil which is current collector and dried in oven at 110°C for 30 min. The dried electrodes were pressed and then dried again in a vacuum oven at 80°C overnight

2.3 Metal dissolution

To investigate the influence of the surface free energy (SFE) on the metal dissolution behavior, one piece of the NCM electrode (14 mm diameter) was stored with 4ml of electrolyte in a PTFE bottle (Cowie) at 60°C for 14 days. The electrolyte which is composed of 1M LiPF₆ in EC/EMC (3/7 by volume, LG Chem.) is used. The water contamination in the electrolyte is under 10 ppm, and the electrolyte is stored in glove box which is filled with Argon gas. After the high temperature (60°C) storage with NCM electrode, the concentration of metal ion in the electrolyte was analyzed by using atomic absorption spectroscopy (AAS, Shimadzu). At the same time, contents of water and HF were analyzed by Karl Fisher (831 KF coulometer, Metrohm) and acid-base titration methods (848 Titrino plus, Metrohm).

3 Results and discussion

3.1 Metal dissolution and Surface Free Energies of $\text{LiNi}_{0.6}\text{Co}_{0.2}\text{Mn}_{0.2}\text{O}_2$

Strong relationships between metal dissolution and SFEs were confirmed by statistical analysis with Minitab software. By measuring mass changes by the adsorption of known liquids which is water, diiodomethane, formamide, we got a lot of contact angle.

Fig. 6 shows various contact angle of probe liquids. Most of them were high contact angle. Especially, diiodomethane adsorbed more rapidly to the powder cathode than other probe liquids.

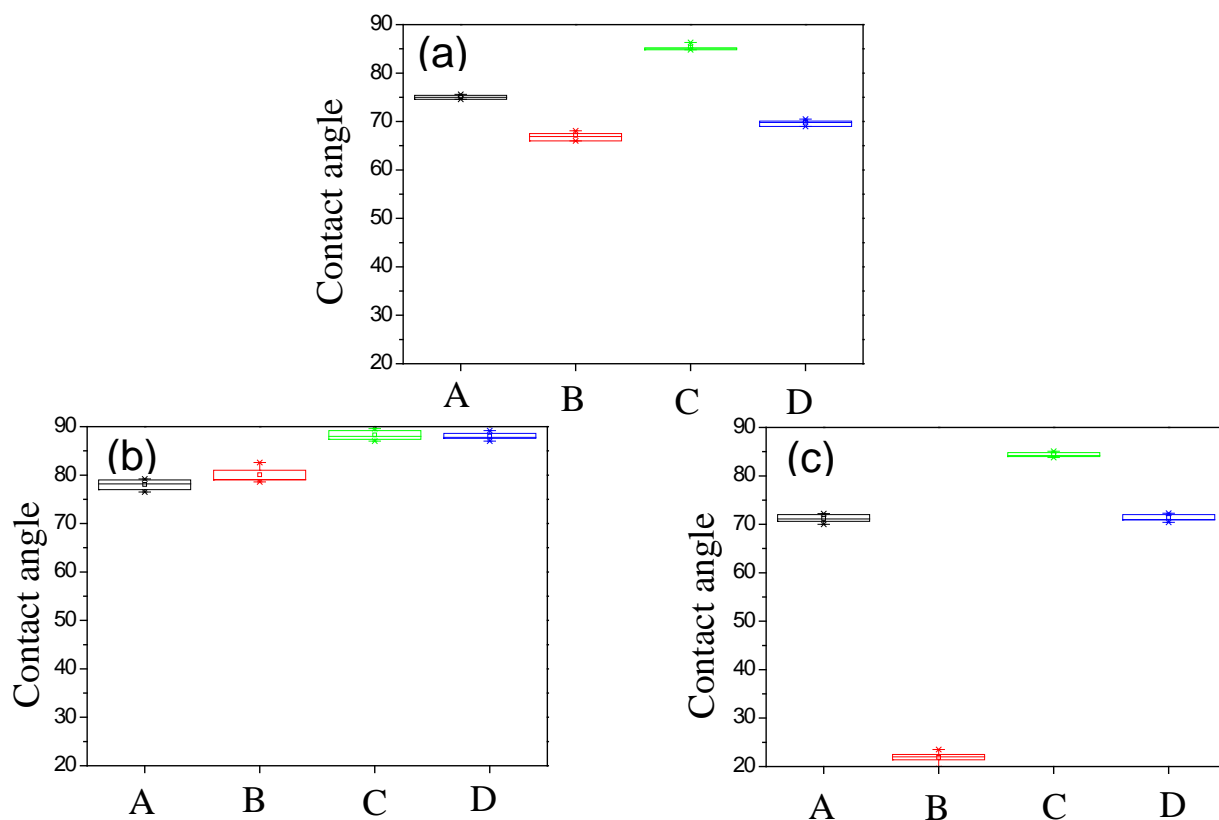


Figure. 6. Contact angle from adsorption method by using (a) water (b) diiodomethane (c) formamide

Fig 7 shows various surface free energy components which is total, dispersity, polarity, acid and base. In general, surface free energy of dispersity showed higher than polarity. Also surface free energy of total, polar and acid components showed same trend. On the contrary, the other showed different trend.

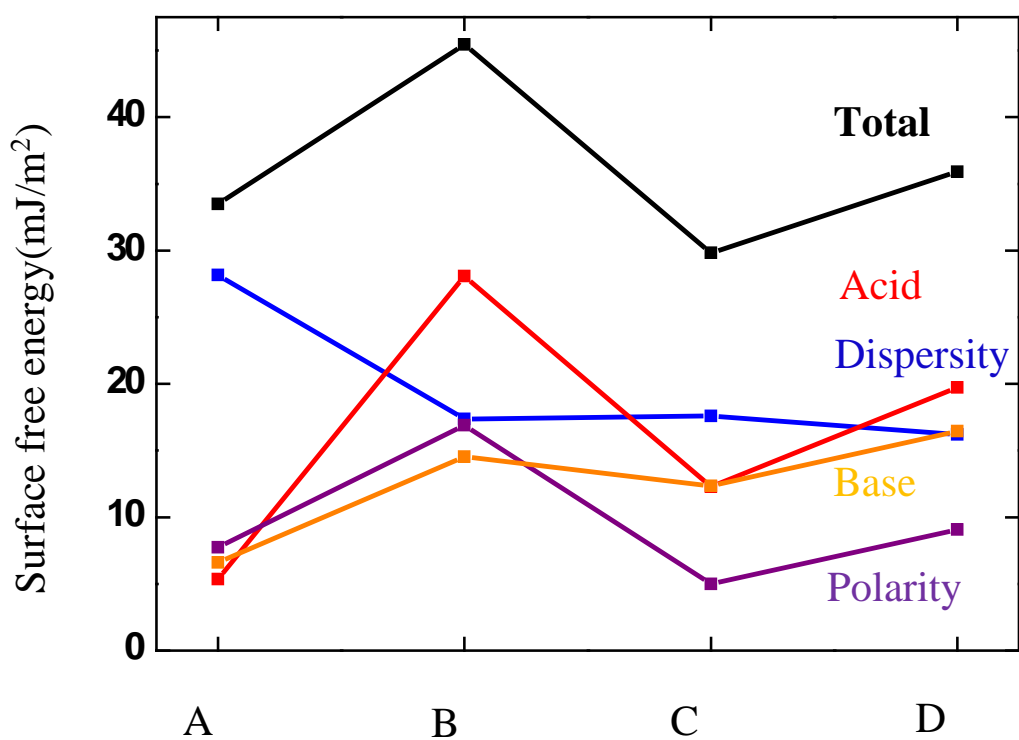


Figure. 7. Surface free energy components

To investigate the correlation of the surface free energy of $\text{LiNi}_{0.6}\text{Co}_{0.2}\text{Mn}_{0.2}\text{O}_2$ with metal dissolution, they were employed at high temperature (60°C) for 14days. Fig 8 shows metal

dissolution of various $\text{LiNi}_{0.6}\text{Co}_{0.2}\text{Mn}_{0.2}\text{O}_2$ electrode.

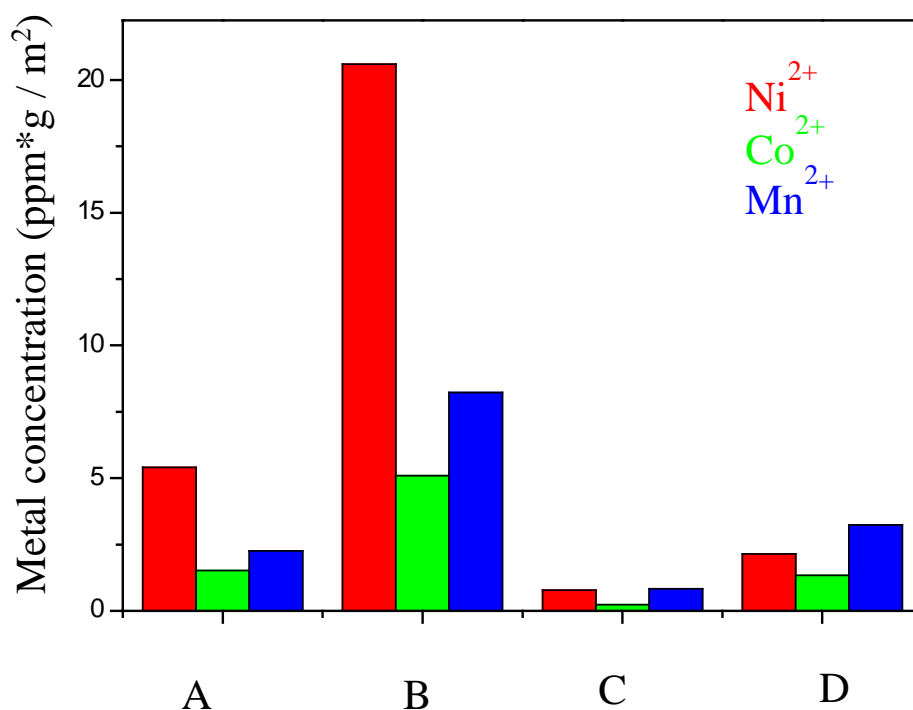


Figure. 8. Mn dissolution of 1M LiPF₆ EC/EMC(3:7) after high temperature (60 °C) storage for 14days.

3.2 Analysis of the morphology of Al coated $\text{LiNi}_{0.6}\text{Co}_{0.2}\text{Mn}_{0.2}\text{O}_2$

To investigate the morphology of $\text{LiNi}_{0.6}\text{Co}_{0.2}\text{Mn}_{0.2}\text{O}_2$, various powders are analyzed using SEM. Fig 9 shows that surface of $\text{LiNi}_{0.6}\text{Co}_{0.2}\text{Mn}_{0.2}\text{O}_2$ were well covered with Al_2O_3 evenly.

Also we confirmed that particle size were correct predictably.

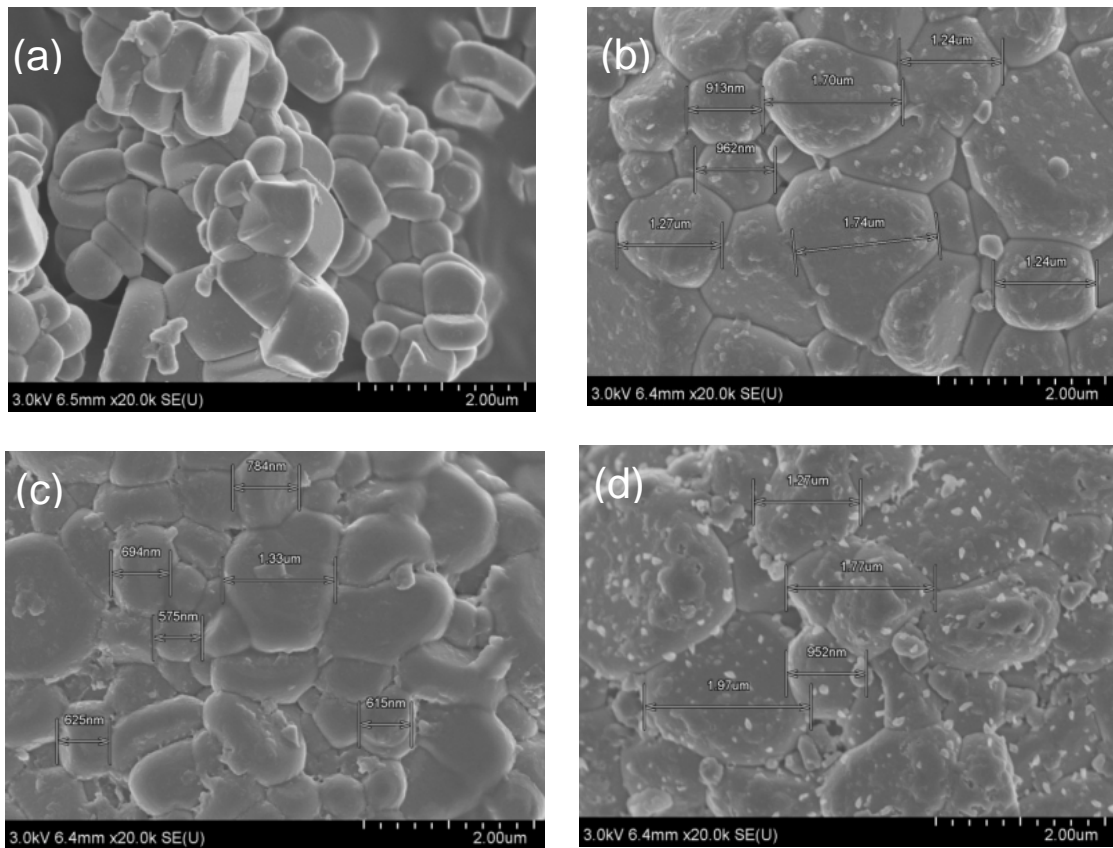


Fig. 9. SEM images of $\text{LiNi}_{0.6}\text{Co}_{0.2}\text{Mn}_{0.2}\text{O}_2$ powders by increasing particle size (a) 4 μm , (b) 10 μm , (c) 10 μm , and (d) 15 μm

3.3 Connection between SFE and metal dissolution of Al coated $\text{LiNi}_{0.6}\text{Co}_{0.2}\text{Mn}_{0.2}\text{O}_2$

Fig 10 shows that the correlations of Ni dissolution with surface free energy. To analyze the results quantitatively, statistical analysis which is correlation coefficient and P-value were used. Table 3. Shows statistical analysis of correlation of Ni dissolution with SFEs. In this case, if the correlation coefficient value closed to 1 which means it has positive linear correlation, and P-value under 0.05 has same meaning.

The P-value of acid with Ni dissolution was 0.05 which means that they have very strong correlation. And total SFE with Mn dissolution showed 0.06 of P-value. But between dispersity of surface free energy and Ni dissolution showed 0.9 of P-value which means that they have no correlation. We confirmed that there are very strong correlation between acid, total surface free energy and Ni dissolution.

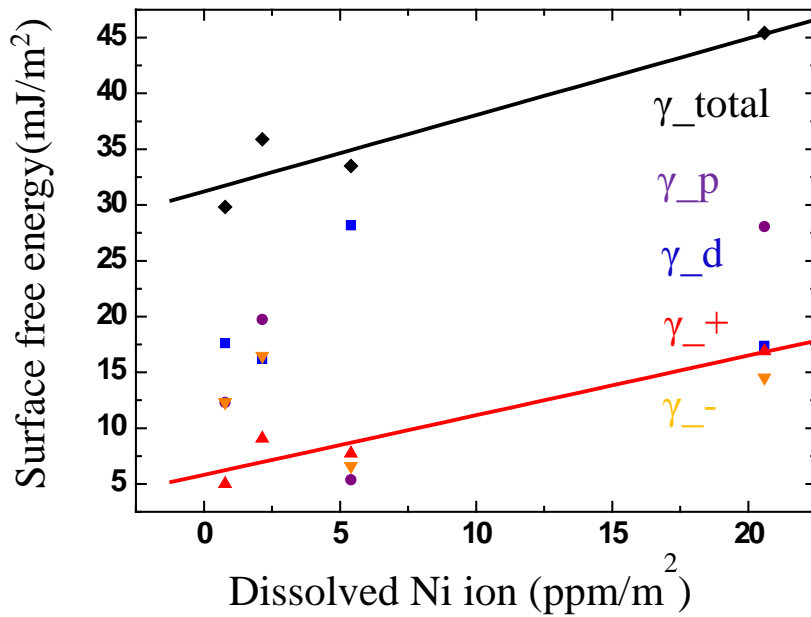


Fig. 10. Correlations of SFEs and Ni dissolution of LiNi_{0.6}Co_{0.2}Mn_{0.2}O₂

	Dispersity (γ_d)	Polarity (γ_p)	Acid (γ_+)	Base (γ_-)	SFE total (γ_{total})
Correlation coefficient	-0.1	0.69	0.95	0.16	0.94
P-value	0.9	0.31	0.05	0.84	0.06

Table. 3. Correlations of SFEs and Ni dissolution of LiNi_{0.6}Co_{0.2}Mn_{0.2}O₂ by using correlation coefficient and P-value

Correlations of Co dissolution of LiNi_{0.6}Co_{0.2}Mn_{0.2}O₂ with SFEs were shown in Fig 11 and Table 4. Between Pp-value of acid surface free energy and Co dissolution was 0.01 which means that they have very strong correlation. And total SFE with Co dissolution showed 0.02 of P-value. But between dispersity of surface free energy and Co dissolution showed 0.85 of P-value. But between dispersity of surface free energy and Co dissolution showed 0.85 of P-value which means that they have no correlation. We confirmed that there are very strong

correlation between acid, total surface free energy and Co dissolution.

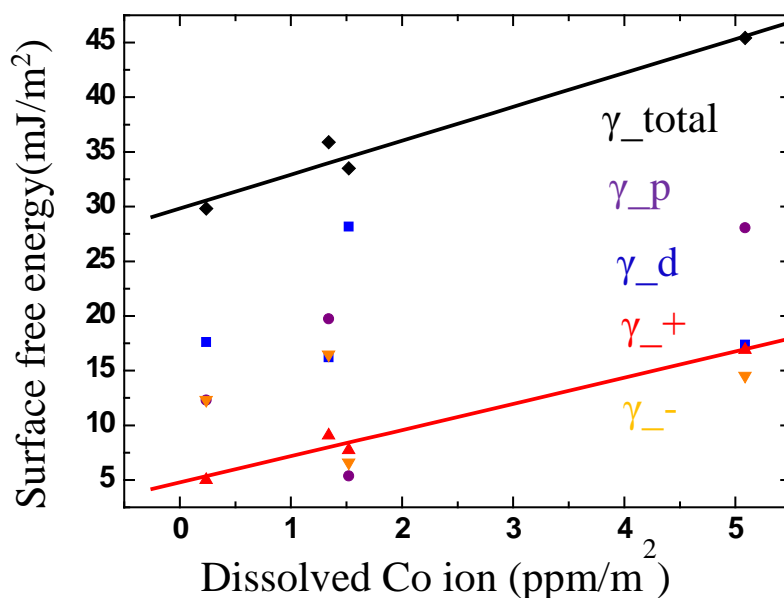


Fig. 11. Correlations of SFEs and Co dissolution of LiNi_{0.6}Co_{0.2}Mn_{0.2}O₂

	Dispersity (γ_d)	Polarity (γ_p)	Acid (γ_+)	Base (γ_-)	SFE total (γ_{total})
Correlation coefficient	-0.15	0.75	0.99	0.25	0.98
P-value	0.85	0.25	0.01	0.75	0.02

Table. 4. Correlations of SFEs and Co dissolution of LiNi_{0.6}Co_{0.2}Mn_{0.2}O₂ by using correlation coefficient and P-value

Correlations of Mn dissolution of LiNi_{0.6}Co_{0.2}Mn_{0.2}O₂ with SFEs were shown in Fig 12 and Table 5. Between P-value of acid surface free energy and Mn dissolution was 0.01 which means that they have very strong correlation. And total SFE with Mn dissolution showed 0.01 of P-value. But between dispersity of surface free energy and Mn dissolution showed 0.73 of P-value which means that they have no correlation. We confirmed that there are very

strong correlation between acid, total surface free energy and Mn dissolution. Fig 13 shows

that schematic illustration of $\text{LiNi}_{0.6}\text{Co}_{0.2}\text{Mn}_{0.2}\text{O}_2$ dissolution mechanisms.

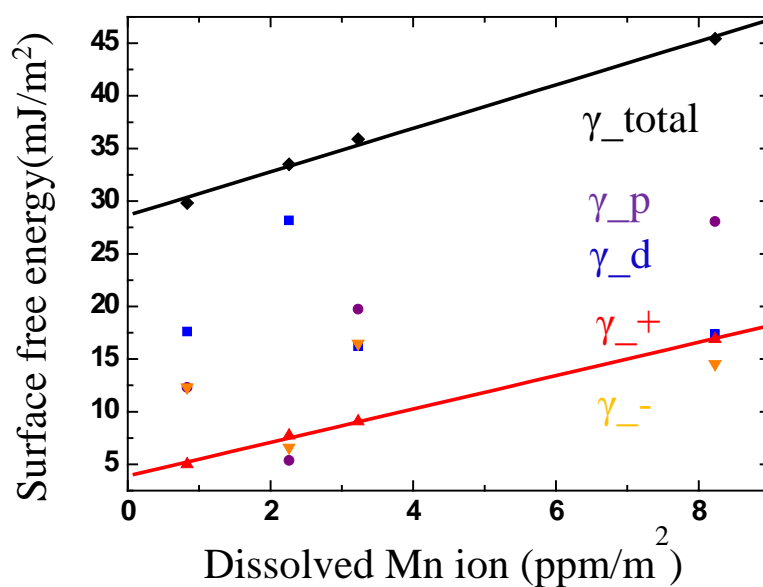


Fig. 12. Correlations of SFEs and Mn dissolution of $\text{LiNi}_{0.6}\text{Co}_{0.2}\text{Mn}_{0.2}\text{O}_2$

	Dispersity (γ_d)	Polarity (γ_p)	Acid (γ_+)	Base (γ_-)	SFE total (γ_{total})
Correlation coefficient	-0.27	0.79	0.99	0.4	0.99
P-value	0.73	0.21	0.01	0.6	0.01

Table. 5. Correlations of SFEs and Mn dissolution of $\text{LiNi}_{0.6}\text{Co}_{0.2}\text{Mn}_{0.2}\text{O}_2$ by using correlation coefficient and P-value

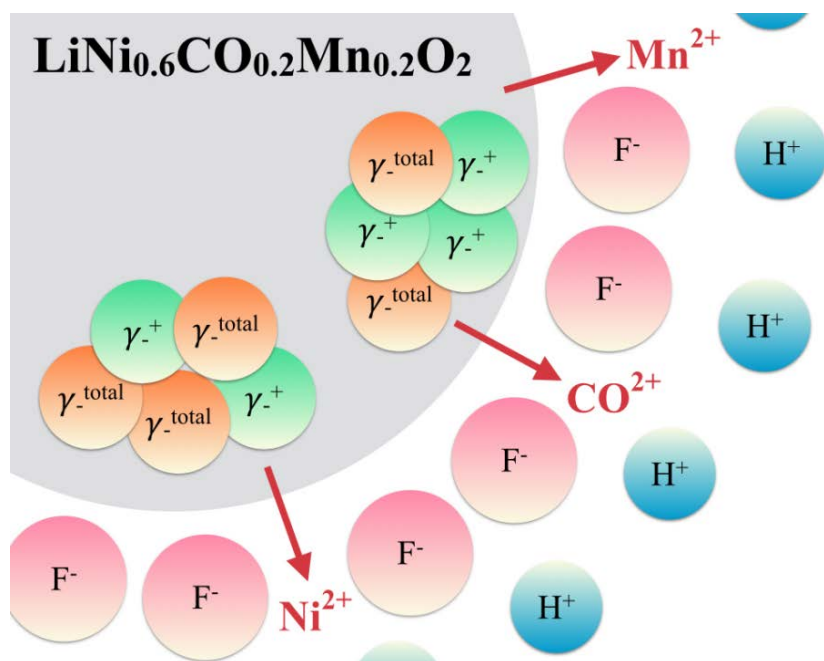


Fig. 13. Schematic illustration of $\text{LiNi}_{0.6}\text{Co}_{0.2}\text{Mn}_{0.2}\text{O}_2$ dissolution mechanisms

4. Conclusions

The SFEs of various kinds of NCM cathode materials for LIBs were analyzed in conjunction with their metal dissolution behavior. We confirmed the strong correlation between surface free energy and metal dissolution behavior of the NCM cathode materials: The higher SFEs, the higher metal dissolution. We also confirmed that the acid and total component ra-

ther than the disperse one dominantly determine the metal dissolution of NCM cathode materials. The acidic part of the polarity of NCM cathode materials is related to the reactivity with F^- ions and the basic one to the reactivity toward H^+ ions in the electrolyte. This study suggests that the SFE characterization of the cathode materials can predict their metal dissolution behavior, and can be an optimization criterion of cathode surface coating materials.

II. Influence of the electrolyte constitution on the dissolution kinetics of manganese from LiMn_2O_4 cathode for lithium ion battery

1 Introduction

Spinel cathode material which is LiMn_2O_4 is considered a promising cathode material for lithium ion batteries, due to its superior electrochemical performance, low cost, and environmental inertness. Especially it is important for large scale applications such as electric vehicles and energy storage systems [19, 20]. However, the poor thermal stability of LMO and manganese dissolution at elevated temperatures has interrupted its progress in new applications [21-30]. In general Mn dissolution is associated with a disproportionation which liberates soluble Mn^{2+} into electrolyte: $\text{Mn}^{3+}(\text{electrode}) \rightarrow \text{Mn}^{4+}(\text{electrode}) + \text{Mn}^{2+}(\text{electrolyte})$ [23-26]. Then, the dissolved Mn^{2+} moves to the anode and aggravates degradation of the anode/electrolyte interface, which is revealed to be a key failure mechanism of LMO-based LIBs at elevated temperature [27-30]. Fig. 14 show that schematic illustration of Mn dissolution. Mn dissolution is heavily affected by electrolyte due to electrode/electrolyte interfacial phenomenon.

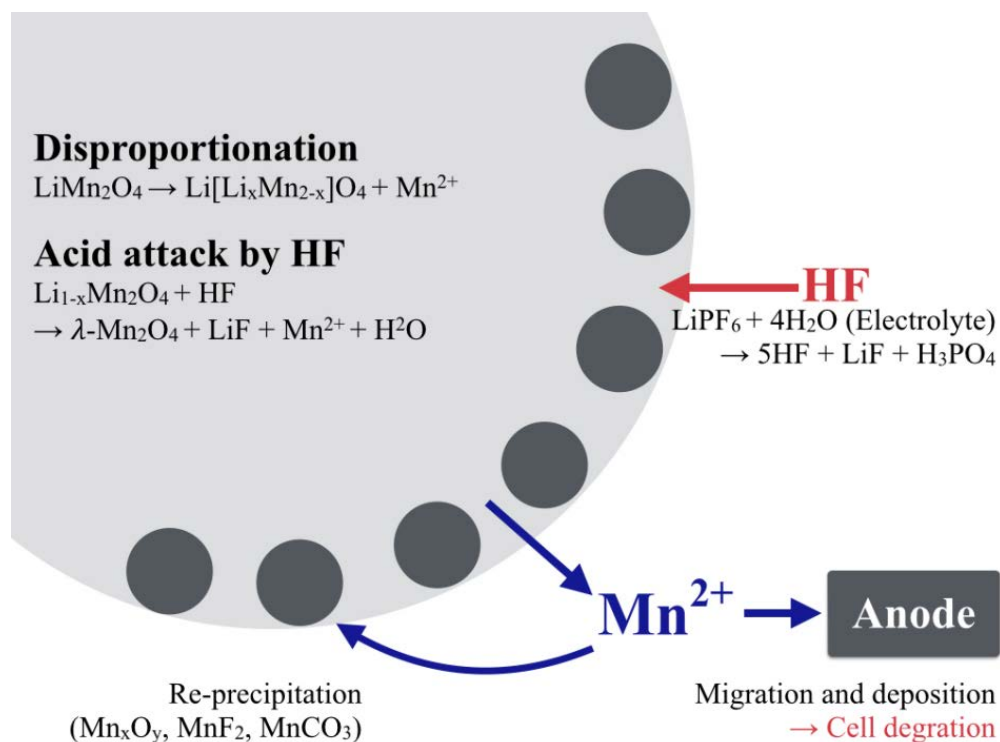


Fig. 14. Schematic illustration of Mn dissolution mechanisms.

However, more detailed research about the relationship between the electrolyte property and Mn-dissolution has not been carried out so far. Therefore, to investigate the effects of electrolyte on the Mn dissolution, the various change in electrolyte compositions based on 1 M LiPF₆ EC/EMC (1/2, v/v), such as different EC content (10, 30, 90 vol. %), were employed for Mn dissolution experiments. Also to investigate the activation energy of electrode/electrolyte interface, different temperature were employed for Mn dissolution experiments. In generally, it is well-known that Mn dissolution behavior arises more severely at elevated temperature, so the samples were stored at 35°C, 45°C, 55°C and 65°C and then

the amount of dissolved Mn ion in the electrolyte was analyzed by Atomic absorption spectroscopy (AAS).

For this systems, two reaction models can be considered [31] model A is unreacted core model for spherical particles with fixed size. Also model B is shrinking core model. Blyr et al. reported that manganese dissolution lead to converted materials whereas the first materials still in the core. [32] So model A likes to be more suitable for explaining the dissolution of manganese ion.

Various established models, i.e., the penetration of soluble Mn^{2+} ions controlled process, chemical reaction controlled process and diffusion controlled process through the product layer. The equations of these models are expressed for various rate controlling mechanism. [30, 33]

1. The penetration of soluble Mn^{2+} ions through electrolyte controlled

$$X_a = kt \quad \text{for mechanism} \quad (\text{Eq. 17})$$

2. Chemical reaction controlled

$$1 - (1 - X_a)^{1/3} = kt \quad \text{for mechanism} \quad (\text{Eq. 18})$$

3. Diffusion controlled through the product layer

$$1 - (1 - X_a)^{2/3} + 2(1 - X_a) = kt \quad \text{for mechanism} \quad (\text{Eq. 19})$$

First mechanism is the penetration of soluble Mn^{2+} ions through electrolyte controlled process. The cause of dissolution $LiMn_2O_4$ is the penetration through electrolyte surrounding particles. Fig 15 shows that schematic diagram controlled by dissolution reaction $LiMn_2O_4$ in electrolyte. Second mechanism is the Chemical reaction controlled process. According to this model, the reaction in the spherical particle occurs homogeneously in all direction. Fig 16 shows that schematic diagram controlled by chemical reaction $LiMn_2O_4$ in electrolyte. Fig 17 show that schematic diagram controlled by diffusion through the product layer $LiMn_2O_4$ in electrolyte for EC/EMC ratio changes (EC=10, 30, 90%).

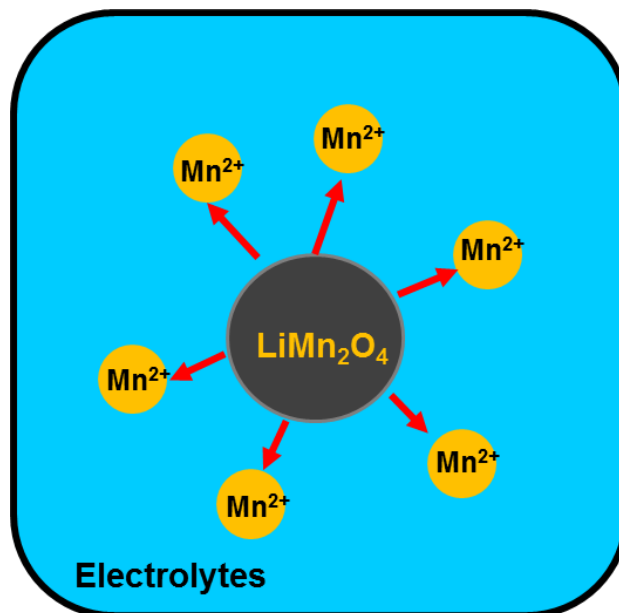


Fig. 15. Schematic diagram controlled by dissolution reaction $LiMn_2O_4$ in electrolyte for EC/EMC ratio changes (EC=10, 30, 90%).

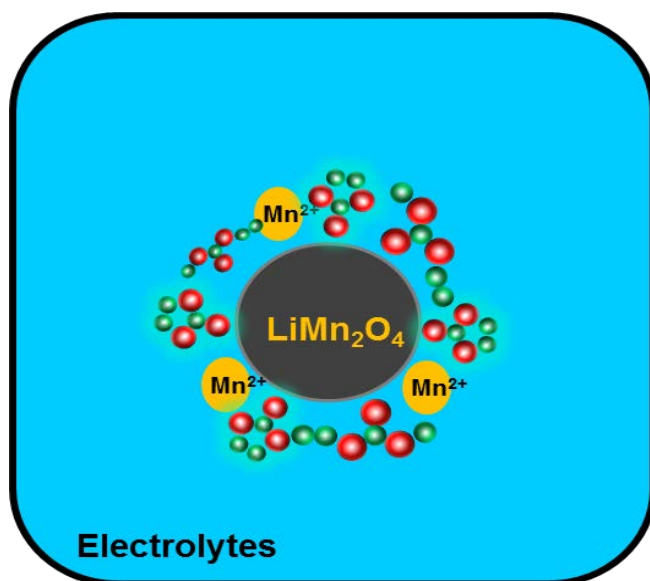


Fig. 16. Schematic diagram controlled by chemical reaction LiMn_2O_4 in electrolyte for EC/EMC ratio changes (EC=10, 30, 90%).

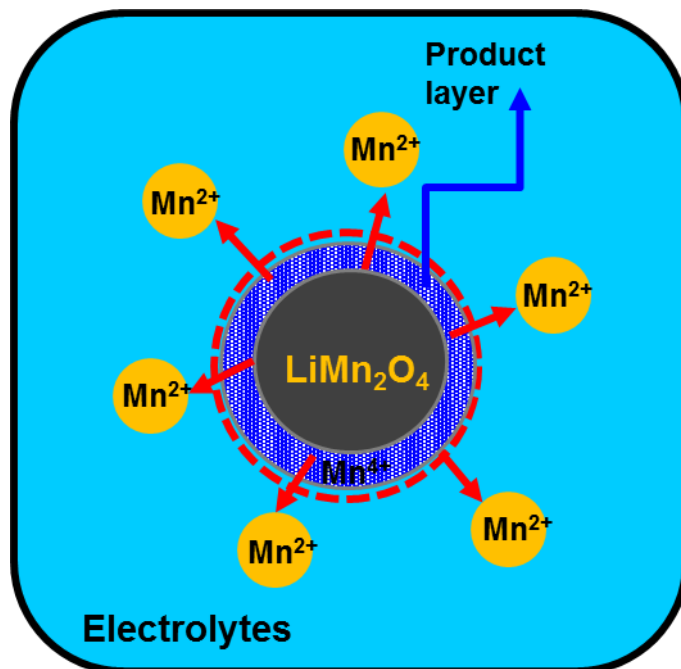


Fig. 17. Schematic diagram controlled by diffusion through the product layer LiMn_2O_4 in electrolyte for EC/EMC ratio changes (EC=10, 30, 90%).

2 Experimental

To analyze the Mn dissolution behavior, each piece of the LMO electrode (14 mm diameter, LMO: PVdF : Super-p=94:3:3, 9.07 ± 0.1 mg/cm², L&F) were stored in a polytetrafluoroethylene (PTFE) bottle with 4 ml of the electrolyte at various temperature (35°C, 45°C, 55°C and 65°C). The weights of the closed PTFE bottles before and after the storage were checked in order to avoid possible errors by leakage during the storage. And the next analysis was performed only when the weight loss was negligible. For determination of dissolved Mn²⁺ concentration, 0.5 ml of electrolyte was sampled and diluted with distilled water by a factor of 10, and then the diluted solution was analyzed by atomic absorption spectroscopy (AA-7000, Shimadzu). At the same time, water and HF contents were analyzed by Karl Fisher (831 KF coulometer, Metrohm) and acid-base titration methods (848 Titrino plus, Metrohm), respectively. Fig. 18 shows the procedure of Mn dissolution experiment.

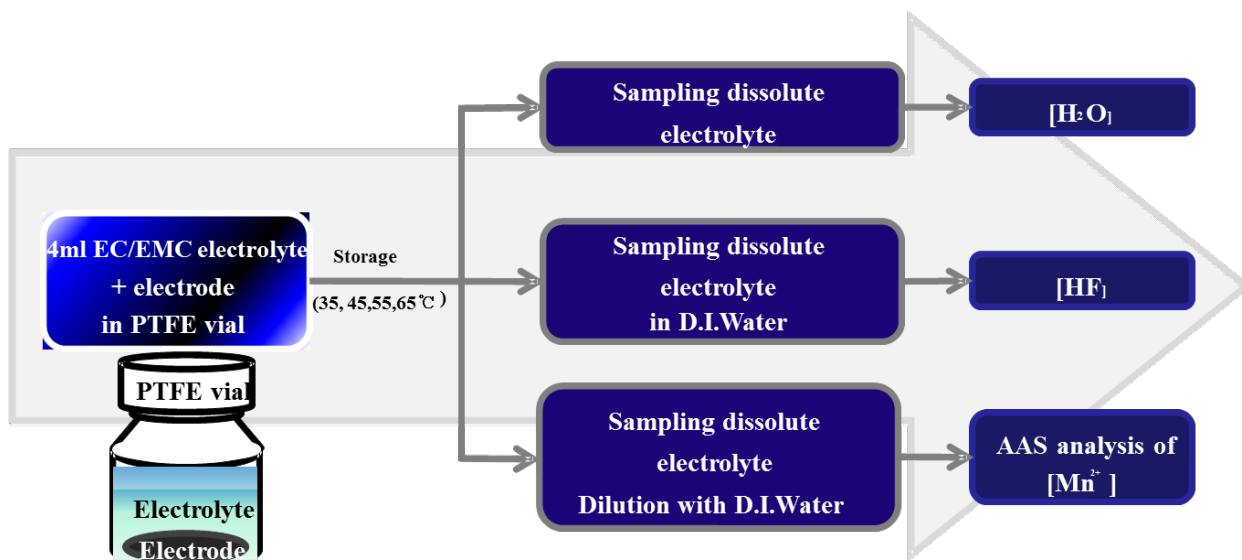


Fig. 18. Procedure of Mn dissolution experiment to investigate the content of water and HF, and the concentration of dissolved Mn^{2+} ion in the electrolyte at various temperature storage (35°C, 45°C, 55°C and 65°C).

3 Results and discussion

3.1 Effects of EC content, reaction temperature and storage time on Mn dissolution

To analyze the effect of EC content on Mn dissolution, the LMO electrodes were stored in electrolyte with different EC contents (10, 30, 90 vol. %) at various temperature for planned days. Also both H₂O and HF of electrolyte were measured simultaneously after each planned days. Fig. 19 show that the amount of Mn²⁺ ion in the electrolyte increases with higher EC content, temperature and storage time. Furthermore, it is indicated that the concentration of Mn²⁺ ion in the electrolyte is saturated after 40 days.

Various temperatures (35°C, 45°C, 55°C and 65°C) were considered for the study of kinetics of manganese dissolution in EC/EMC. Especially, contents of manganese dissolution were more than other temperatures at 65°C. Based on the saturated state, more consideration about kinetics and activation energy of Mn dissolution will be discussed.

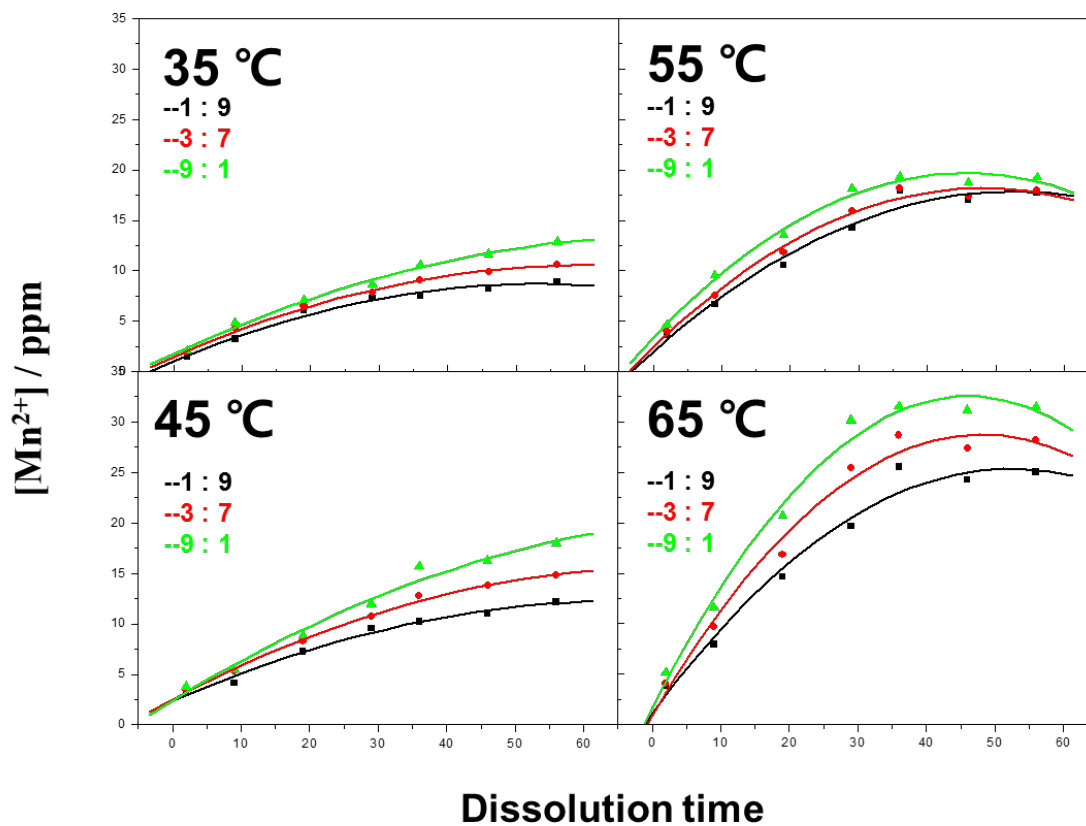


Fig. 19. Mn dissolution of 1 M LiPF₆ EC/EMC (1/9, 3/7, 9/1 by volume) at various temperature (35°C, 45°C, 55°C and 65°C) storage for 2, 9, 19, 29, 36, 46 and 56 days.

3.2 Kinetics of Mn dissolution

By means of the relationship between the dissolution amount and the storage time at various temperature, the dissolution mechanism of the LiMn_2O_4 system can be further explored by kinetic analysis. In the dissolution reaction of LiMn_2O_4 , Mn^{3+} ions first convert into Mn^{2+} ions and then diffuse into the electrolytes. The dissolution reaction can be considered to take place in a liquid-solid system. The particles were suppose to be homogeneous spherical solid phase. It was selected to analyze the dissolution rate of manganese in solution.

3.3 The penetration of soluble Mn^{2+} ions through electrolyte controlled process

Firstly, the conversion of the dissolution reaction (X_a) was calculated from Eq.17, 20 where the Mn^{2+} in the numerator was obtained from the data in Fig. 19. Fig 20 showed that nonlinear tendencies with R^2 values of 0.968, 0.983 and 0.988 for EC/EMC ratio changes (EC=10, 30, 90%) at 35°C respectively. At 45°C, it showed that nonlinear tendencies with R^2 values of 0.988, 0.983 and 0.979 for EC/EMC ratio changes (EC=10, 30, 90%) respectively. The R^2 values for EC/EMC ratio changes (EC=10, 30, 90%) are 0.970, 0.987 and 0.978 at 55°C respectively. At 65°C, it showed that nonlinear tendencies with R^2 values of 0.978, 0.979 and 0.978 for EC/EMC ratio changes (EC=10, 30, 90%) respectively. However the reaction rate constant (k) is proportional to the EC contents and the temperature. Fig 14 shows that schematic diagram controlled by dissolution reaction LiMn_2O_4 in electrolyte.

$$X_a = \frac{\text{(dissolved Mn}^{2+} \text{ mole in the electrolyte)} \times 2}{\text{Mn}^{2+} \text{ mole in LMO electrode}} \quad (\text{Eq. 20})$$

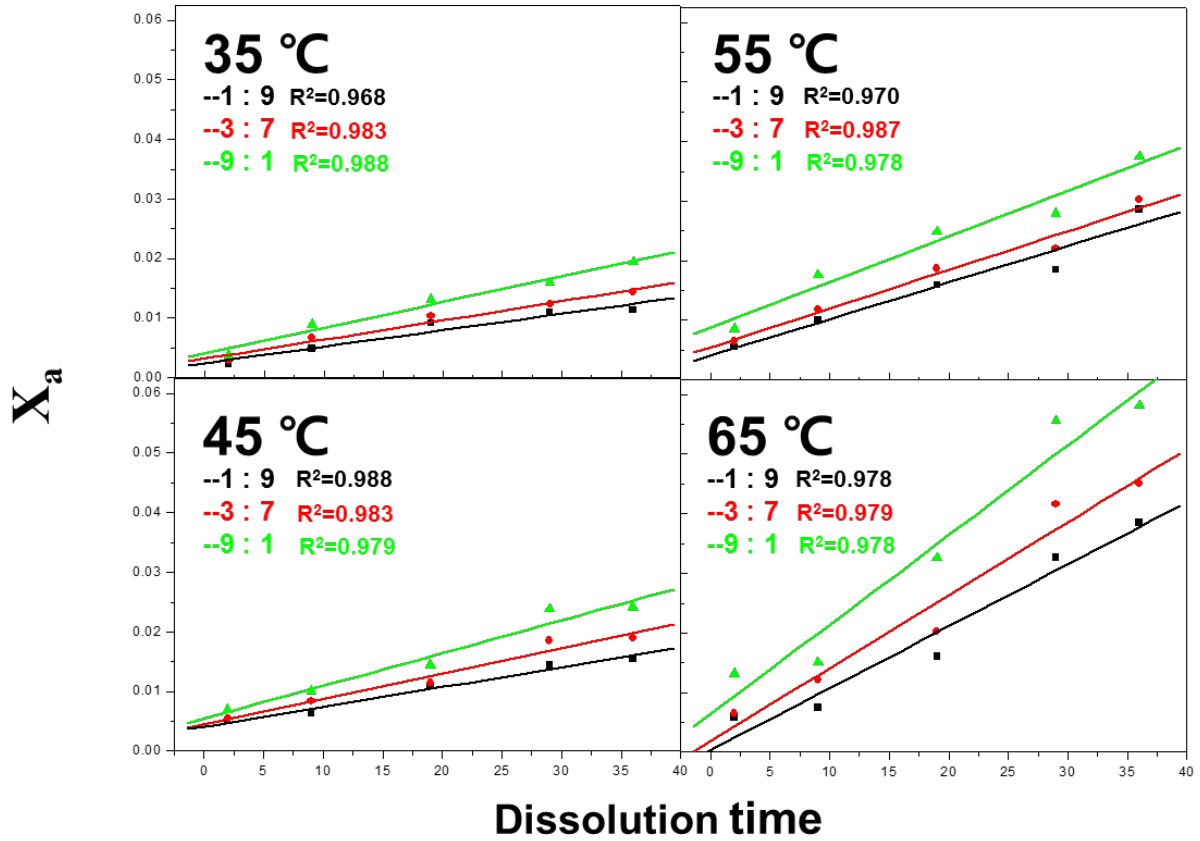


Fig. 20. The penetration of soluble Mn^{2+} ions through electrolyte mechanisms are plotted for various temperatures and EC/EMC ratio changes (EC=10, 30, 90%)

3.4 Chemical reaction controlled process

Time for different fraction of reacted particles of manganese at 35°C, 45°C, 55°C and 65°C were calculated from eq18. Fig 21 shows that the correlation coefficient values of the plotted lines. The correlation factors for the four temperatures were very low. Therefore chemical reaction model could not be the rate determining step during dissolution of manganese. It

showed that nonlinear tendencies with R^2 values of 0.968, 0.983 and 0.988 for EC/EMC ratio changes (EC=10, 30, 90%) at 35°C respectively. At 45°C, it showed that nonlinear tendencies with R^2 values of 0.988, 0.983 and 0.964 for EC/EMC ratio changes (EC=10, 30, 90%) respectively. The R^2 values for EC/EMC ratio changes (EC=10, 30, 90%) are 0.970, 0.987 and 0.978 at 55°C respectively. At 65°C, it showed that nonlinear tendencies with R^2 values of 0.972, 0.979 and 0.978 for EC/EMC ratio changes (EC=10, 30, 90%) respectively. However the reaction rate constant (k) is proportional to the EC contents and high temperature.

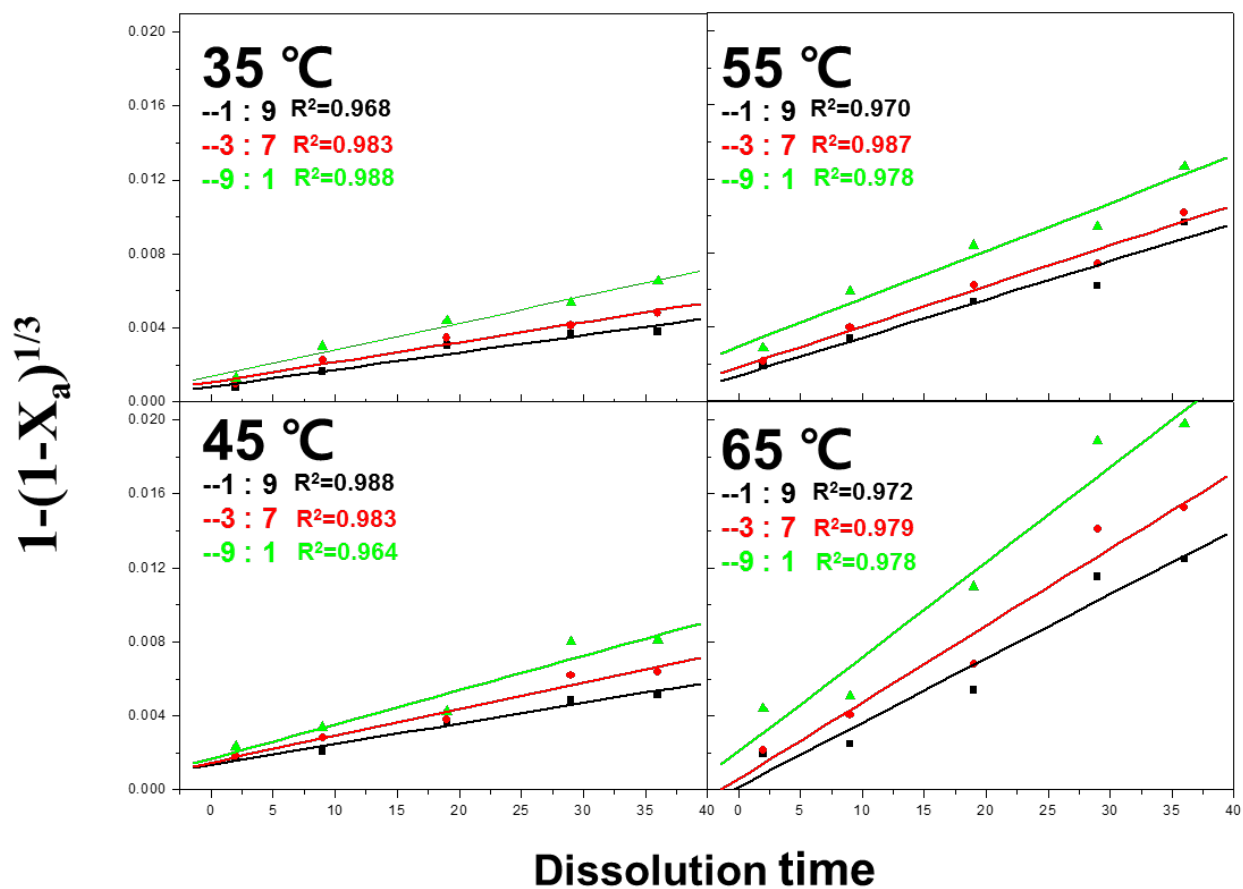


Fig. 21. Chemical reaction mechanisms are plotted for various temperatures and EC/EMC ratio changes (EC=10, 30, 90%)

3.5 Diffusion controlled through the product layer

Fig 22 illustrates the curves corresponding to the function of $1-(1-X_a)^{2/3}+2(1-X_a) = kt$ at various temperature (35°C, 45°C, 55°C and 65°C) as a function of reaction time. The data yielded a very high correlation coefficient for all the temperature. This model displays good linearity and the correlation coefficient(R). In other words, the rate of manganese dissolution reaction from LiMn_2O_4 is controlled by the diffusion of soluble Mn^{2+} ions through the product layer rather than the chemical reaction and the penetration of soluble Mn^{2+} ions. It is obvious that the data does fit with a straight line and it is concluded that the diffusion through a solid reaction product. Fig 22 shows that linear tendencies with R^2 values of 0.985, 0.998 and 0.990 for EC/EMC ratio changes (EC=10, 30, 90%) at 35°C respectively. At 45°C, it showed that linear tendencies with R^2 values of 0.989, 0.988 and 0.979 for EC/EMC ratio changes (EC=10, 30, 90%) respectively. The R^2 values for EC/EMC ratio changes (EC=10, 30, 90%) are 0.975, 0.994 and 0.995 at 55°C respectively. At 65°C, it showed that linear tendencies with R^2 values of 0.969, 0.985 and 0.986 for EC/EMC ratio changes (EC=10, 30, 90%) re-

spectively. So the reaction rate constant (k) is proportional to the EC contents and high temperature.

According to Eq. 19, the reaction rate constant k can be calculated from the slope of each line in Fig 18. When the EC/EMC ratio changes (EC=10, 30, 90%) the reaction rate constants (k) are 1.32×10^{-6} , 1.90×10^{-6} and $3.43 \times 10^{-6} \text{s}^{-1}$ at 35°C respectively. At 45°C , the reaction rate constants (k) are 2.28×10^{-6} , 3.69×10^{-6} and $6.71 \times 10^{-6} \text{s}^{-1}$ respectively. The reaction rate constants (k) are 6.76×10^{-6} , 7.87×10^{-6} and $1.24 \times 10^{-5} \text{s}^{-1}$ for 55°C respectively. At 65°C , the reaction rate constants (k) are 1.39×10^{-5} , 2.09×10^{-5} and $3.62 \times 10^{-5} \text{s}^{-1}$ respectively. It means k value increase with higher EC contents and temperature.

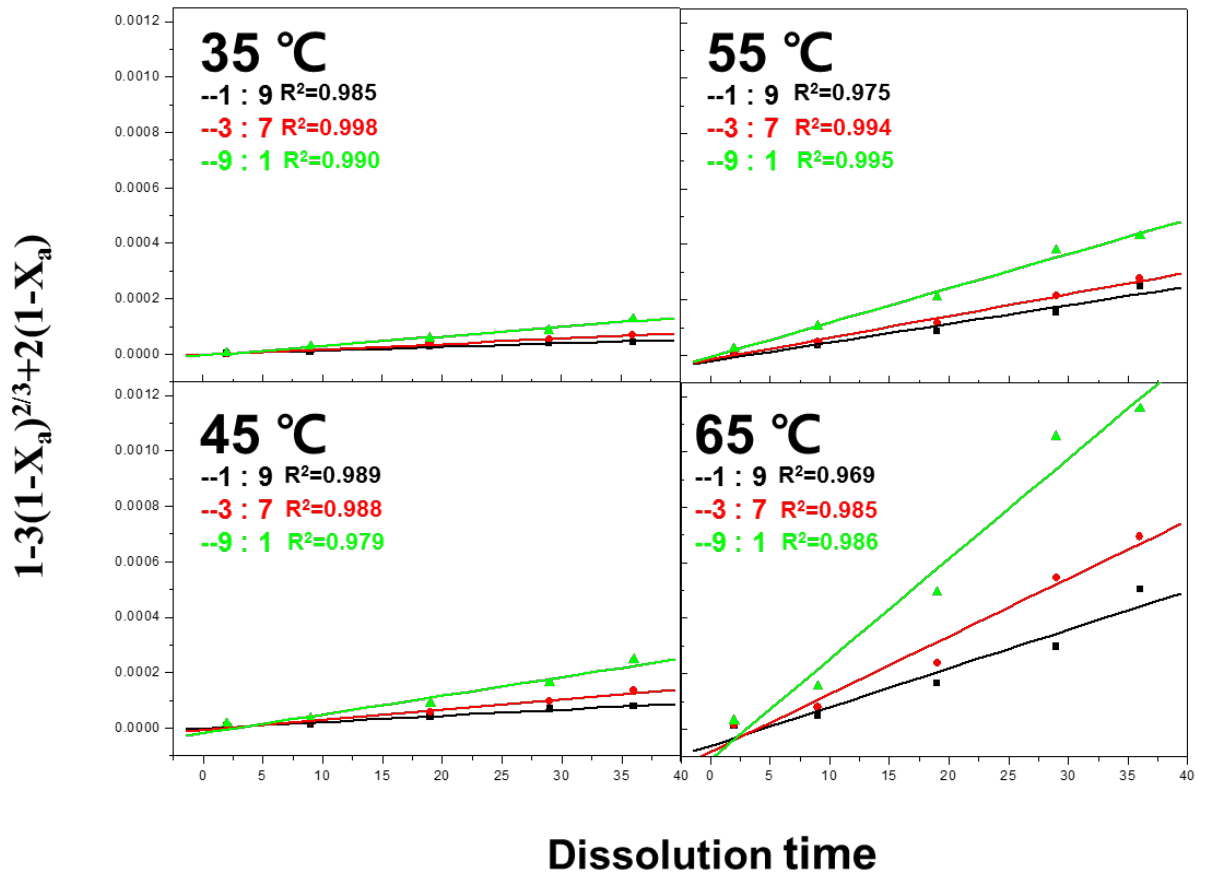


Fig. 22. Diffusion through the product layer mechanisms are plotted for various temperatures and EC/EMC ratio changes (EC=10, 30, 90%).

3.6 Activation energy determination

Reaction rate constants (k) at various temperatures were obtained from the slope of the linear plots for manganese. And then the values of reaction rate constants (k) were plotted according to the Arrhenius type equation. Fig 23-25 shows that the plot of $\ln K$ vs. $1/T$ (K) was straight line for manganese. The apparent activation energy calculated from the Arrhenius plot was 70.5 kJ/mol for EC/EMC ratio (1:9). For EC/EMC ratio (3:7) and (9:1), the magnitudes of activation energy are calculated to be 68.5, 65.3 kJ/mol. The more EC contents increase, the less activation energy decrease. These results confirmed that manganese dissolution is controlled by diffusion through the product layer.

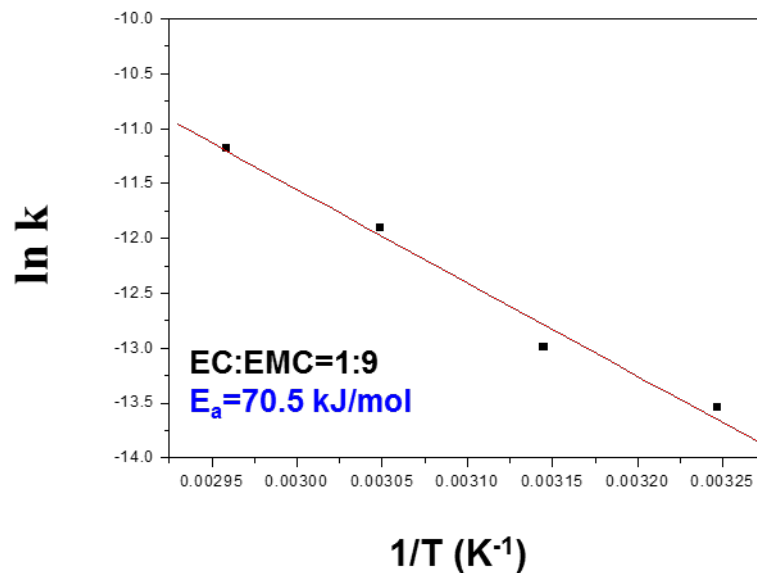


Fig. 23. Arrhenius plot for the dissolution of manganese for EC/EMC ratio (1:9)

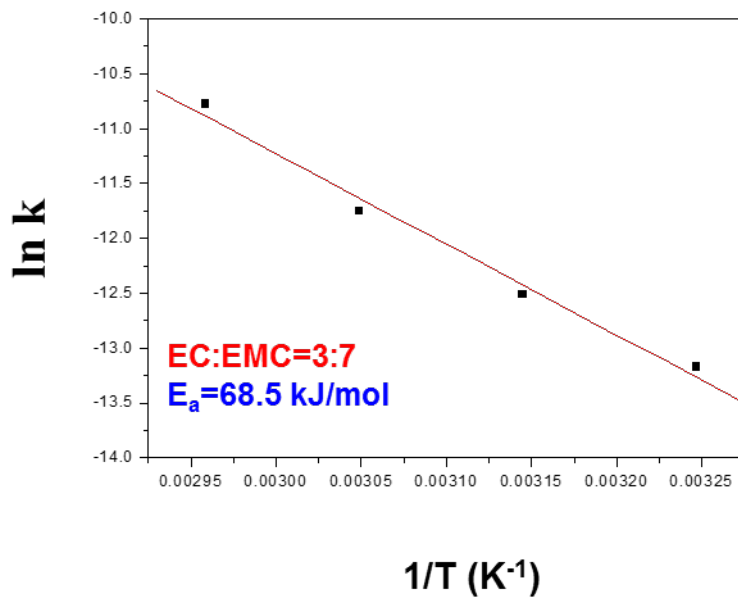


Fig. 24. Arrhenius plot for the dissolution of manganese for EC/EMC ratio (3:7)

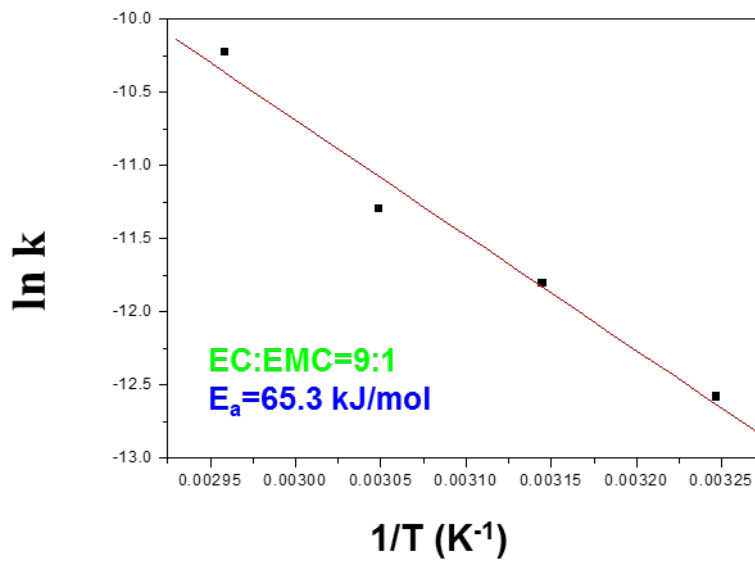


Fig. 25. Arrhenius plot for the dissolution of manganese for EC/EMC ratio (9:1)

3.7 Effect of solvation energy and HF

Mn dissolution experiment with various salts (LiPF_6 , LiClO_4 , LiTFSI) solvents and HF Contents were used in this study.

Particularly, the lithium bis(trifluoromethylsulfonyl)imide(LiTFSI) salt is well known to be more stable and safer than the LiPF_6 salt. [36] Other solvents are ethyl methyl carbonate (EMC), ethyl carbonate (EC), 1,2-dimethoxyethane (1G), Trimethyl phosphate (TMP), and dimethyl sulfoxide (DMSO). 1 M LiPF_6 X/EMC (1:1 by mol, X=EMC, EC, 1G, TMP or DMSO) were stored at 60°C oven for 7 days with a piece of LMO electrode. Fig. 26-28 show that the Mn dissolution is exponentially proportional to the donor number (DN) of solvents. The DN is a quantitative measure of the ability to solvate cations and Lewis acids. Considering donor number represents solvation energy, the experimental result that the Mn dissolution is exponentially proportional to the donor number of the solvent. To analyze the influence of HF, it was added to LiClO_4 , LiTFSI solution. Also, Fig. 26-27 show the contents of Mn dissolution were proportional to HF.

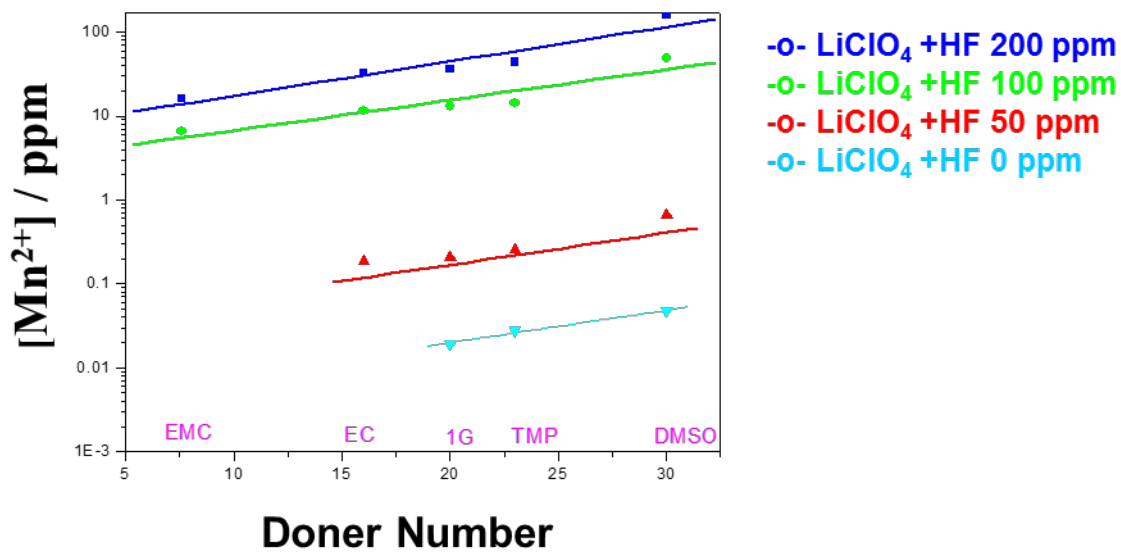


Fig. 26. Mn dissolution of 1M LiClO₄ X/EMC (1:1mol, X=EMC, EC, 1G, TMP or DMSO) for various HF contents.

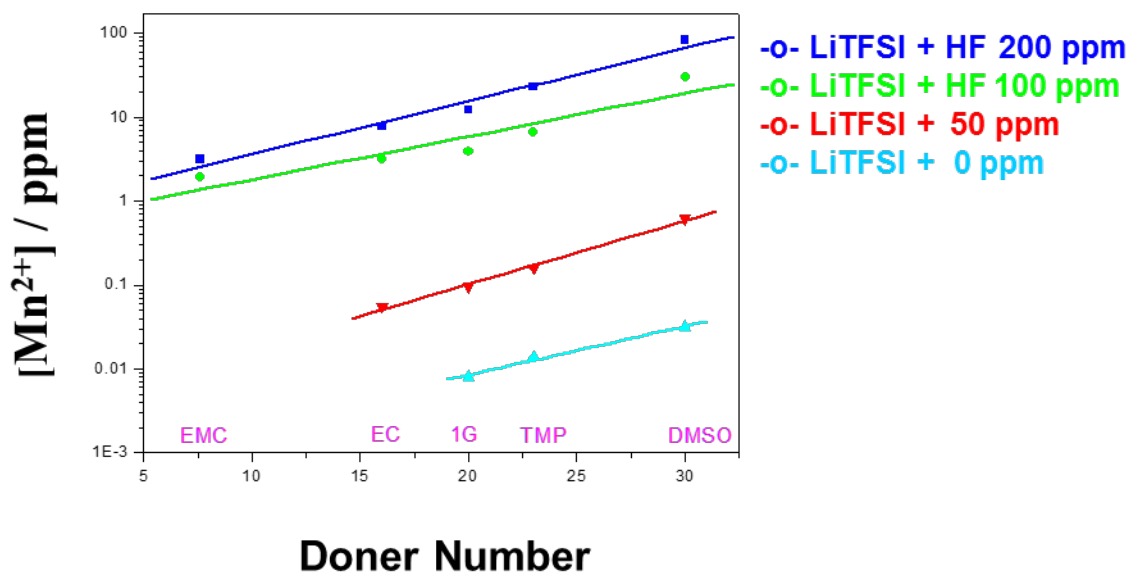


Fig. 27. Mn dissolution of 1M LiTFSI X/EMC (1:1mol, X=EMC, EC, 1G, TMP or DMSO) for various HF contents.

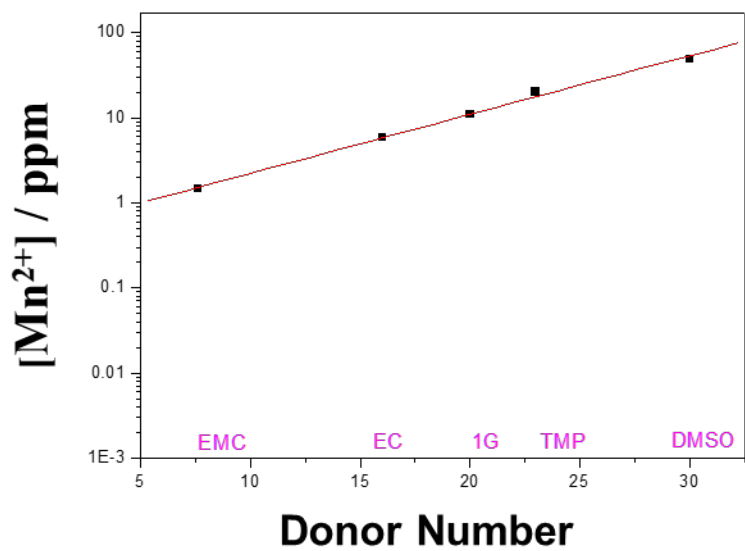


Fig. 28. Mn dissolution of 1M LiPF₆ X/EMC (1:1mol, X=EMC, EC, 1G, TMP or DMSO)

4. Conclusions

We examined the kinetics of manganese dissolution at elevated temperatures, storage duration and EC/EMC ratio changes (EC=10, 30, 90%) from LiMn_2O_4 . Manganese dissolution increased with EC contents and high temperature. Dissolution data showed that manganese dissolution occurs by diffusion reaction of Mn^{2+} ions through the product layer. The rate constant of the diffusion reaction was dependent on EC content. The concentration of Mn ion in the electrolyte was saturated after 40 days. In addition, low EC contents possess a higher activation energy and greater reaction rate constant of the dissolution process. Therefore, the dissolution of manganese from LiMn_2O_4 will be accelerated at elevated temperatures and high EC ratio.

III. Analysis of surface free energy in battery electrolytes

1 Introduction

Li-ion batteries (LIBs) are widely used for large scale applications like electric vehicles and renewable energy storage systems. For a better understanding of the adsorption behavior of liquid electrolyte on electrodes, the interface parameters are determined by contact angle and surface tension measurements. Characterization and expectation of wetting phenomenon by contact angle measurements and surface free energy calculations are powerful analysis tools.

Many factors affect the performances of batteries. One of the key factors is the wettability of both electrodes and electrolytes.

Characterization and prediction of wetting phenomenon by contact angle measurements and surface free energy calculations are excellent analysis tools. The thermodynamics of the sessile drop were first described by Young [34], which establishes the relation between the surface free energies of a liquid and solid. For a better understanding of the adsorption behavior of liquid electrolyte on electrodes, the interface parameters are determined by contact angle and surface tension measurements.

If we know surface free energy of various probe solid, we calculate SFEs of battery electro-

lyte such as propylene carbonate(PC) and dimethyl sulfoxide(DMSO) ethylene carbonate(EC), ethyl methyl carbonate(EMC), dimethyl carbonate(DMC), diethyl carbonate(DEC). Already, we know surface free energy values for wafer, polystyrene and aluminium. On the basis of the contact angles obtained on wafer, polystyrene and aluminium oxide the Lifshitz-van der Waals components of the water, diiodomethane and formamide surface free energy were determined. By using the contact angle values of wafer, polystyrene and aluminium the value of the electron acceptor(γ^+) and electron donor(γ^-) parameters of the acid-base components of battery electrolyte such as propylene carbonate(PC) and dimethyl sulfoxide(DMSO).

Eventually, we can get Lewis acid component or the electron acceptor (γ^+) and Lewis base component or the electron donor (γ^-) component of liquid electrolyte based on SFE of solid surface tension such as wafer, polystyrene, aluminum oxide.

The main purpose is to determine the γ^+ , γ^- and γ^d values of battery electrolyte such as propylene carbonate(PC) and dimethyl sulfoxide(DMSO) by using wafer, polystyrene and aluminium. These results will provide valuable guidance for calculate the surface free energy of electrolyte.

2 Experimental

First we have to calculate the surface free energy of probe solids such as Al_2O_3 , Polystyrene(PS) and Wafer(Si-111). Three probe liquids were used to measure probe solids in order to calculate SFEs. Diiodomethane, formamide (Aldrich) and deionized water were used for probe liquids. Table 6 shows SFE properties of probe liquids. [35]

The liquid surface free energy has been measured from a tensiometer (Kruss, Germany) using the ring method. Between 7 and 10 measurements were performed for each sample. The highest and lowest values were disregarded and the remaining values were used to calculate.

The measurements were done that the vertically hung ring was dipped into the liquid to measure its surface tension. And then it was pulled out. The maximum force needed to pull the ring through the interface was expressed as surface tension γ_L (mN/m). It was first calibrated with pure water to ensure accuracy. The surface free energy of pure water was obtained to be close to 72.5 mJ/m^2 .

And then the contact angles of probe solid were measured according to sessile drop method using a goniometer (Krüss, Germany). The contact angles were measured as soon as the liquids dropped on the probe solids. Fig 29 shows schematics of surface free energy factors be-

tween solid, liquid and vapor. We can get surface free energy of probe solids.

Finally, we can calculate the surface free energy of electrolyte by using vOCG (eq13) equation.

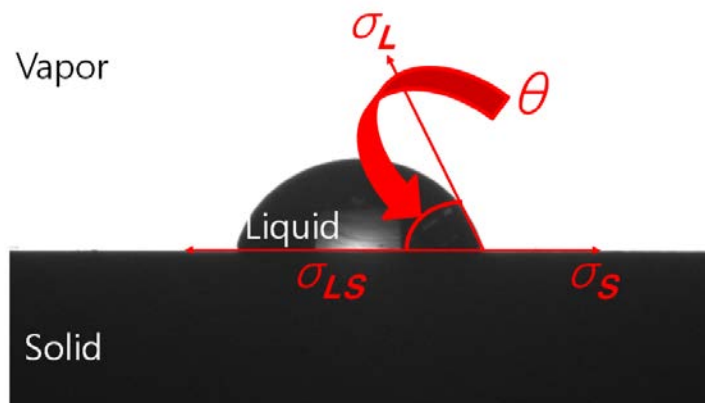


Fig. 29. Schematics of SFEs factors between solid, liquid and vapor

	γ_L	γ_L^d	γ_L^p	γ_L^+	γ_L^-
diiodomethane	50.8	50.8	0	0	0
formamide	58	39	19	2.28	39.6
water	72.8	21.8	51	25.5	25.5

Table 6. SFE properties of probe liquids [35]

3 Results and discussion

3.1 Characterization of reference materials

Contact angle values obtained with the reference liquids water, diiodomethane, and formamide for probe solids such as Al_2O_3 , Polystyrene(PS) and Wafer(Si-111) are displayed in Table 7-9. Table 6 show that water and formamide have both polar and dispersive components, while diiodomethane has mostly dispersive components. Fig. 30-32 show that the contact angle probe liquids such as water, diiodomethane, formamide were displayed on reference materials like Al_2O_3 , Polystyrene(PS) and Wafer(Si-111). Based on contact angle of probe solids, we can calculate the surface free energy of electrolyte.

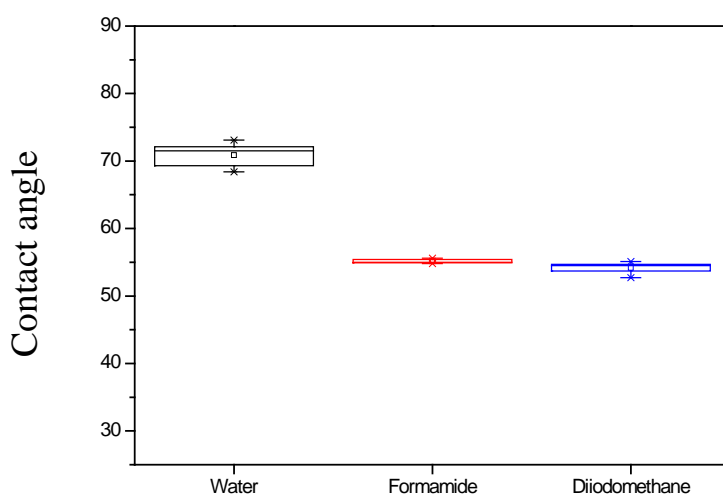


Fig. 30. Contact angle with reference liquids on Al_2O_3

Al ₂ O ₃ (25'c)				
γ_d	γ_P	γ_+	γ_-	γ_{tot}
31.6	4.8	0.4	14.1	36.4

Table.7. Surface free energy and its dispersive, polar, Lewis acid and base components for Al₂O₃ with the vOCG equation.

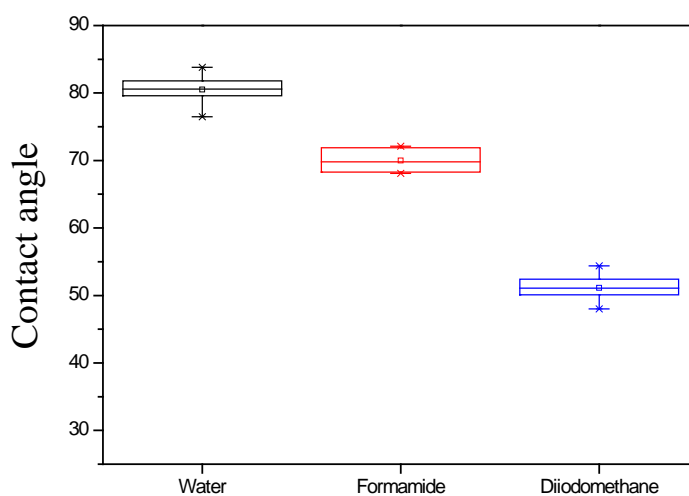


Fig. 31. Contact angle with reference liquids on PS

PS(25'c)				
γ_d	γ_P	γ_+	γ_-	γ_{tot}
33.5	2.6	0.1	11.5	36.3

Table.8. Surface free energy and its dispersive, polar, Lewis acid and base components for PS with the vOCG equation.

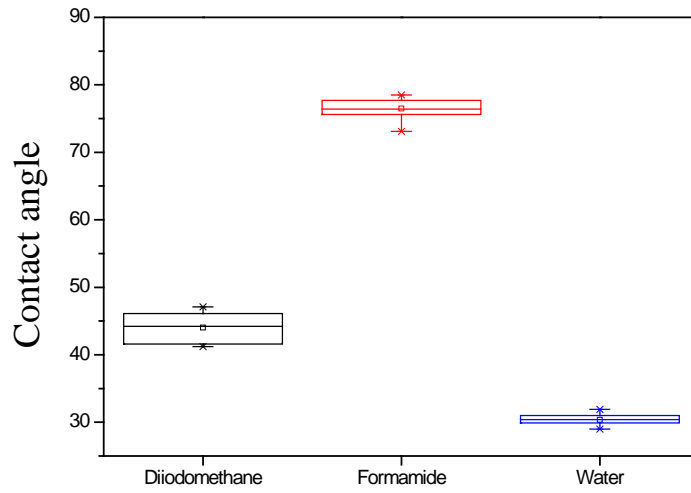


Fig. 32. Contact angle with reference liquids on wafer

Wafer(25°c)				
γ_d	γ_P	γ_+	γ_-	γ_{tot}
31.1	10	1.72	15.25	41

Table.9. Surface free energy and its dispersive, polar, Lewis acid and base components for wafer with the vOCG equation.

3.2 The surface free energy calculation of propylene carbonate and dimethyl sulfoxide

Based on contact angle of probe solids, we calculate the surface free energy of propylene carbonate. Fig. 33 show that the contact angle of propylene carbonate were displayed on reference materials such as Al_2O_3 , Polystyrene (PS) and Wafer (Si-111). Due to we know the surface free energy of probe solids, we can calculate propylene carbonate. Table 10-12 show that the surface free energy of PC by using two probe solids such as PS and Wafer or Wafer, Al_2O_3 or . Al_2O_3 and PS.

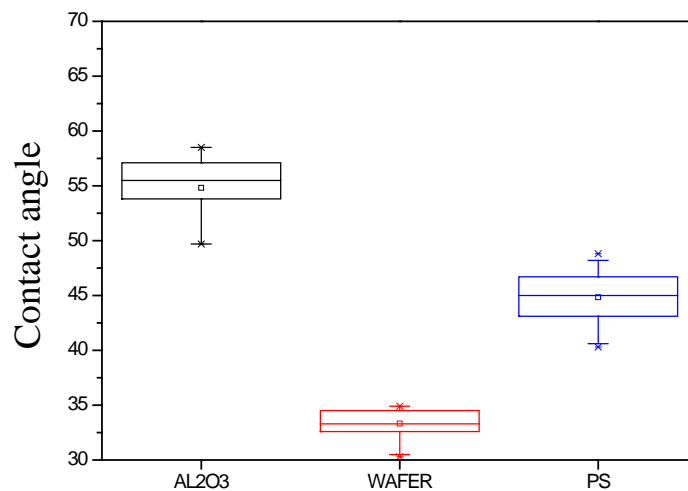


Fig. 33. Contact angle with reference liquids on propylene carbonate

Pure PC(PS, WAFER)				
γ_d	γ_P	γ_+	γ_-	γ_{tot}
14.1	26.6	5.9	29.7	40.9

Table 10. Surface free energy of PC by using 2 probe solids (PS, Wafer)

Pure PC(WAFER, Al ₂ O ₃)				
γ_d	γ_P	γ_+	γ_-	γ_{tot}
19.8	21.3	3.2	35.3	41

Table 11. Surface free energy of PC by using 2 probe solids (Wafer, Al₂O₃)

Pure PC(PS, Al ₂ O ₃)				
γ_d	γ_P	γ_+	γ_-	γ_{tot}
20.8	20.2	16.2	6.29	41

Table 12. Surface free energy of PC by using 2 probe solids (PS, Al₂O₃)

Based on contact angle of probe solids, we calculate the surface free energy of propylene carbonate. Fig. 33 show that the contact angle of propylene carbonate were displayed on reference materials such as Al₂O₃, Polystyrene (PS) and Wafer (Si-111). Due to we know the surface free energy of probe solids, we can calculate propylene carbonate. Table 10-12 show that the surface free energy of PC by using two probe solids such as PS and Wafer or Wafer, Al₂O₃ or . Al₂O₃ and PS.

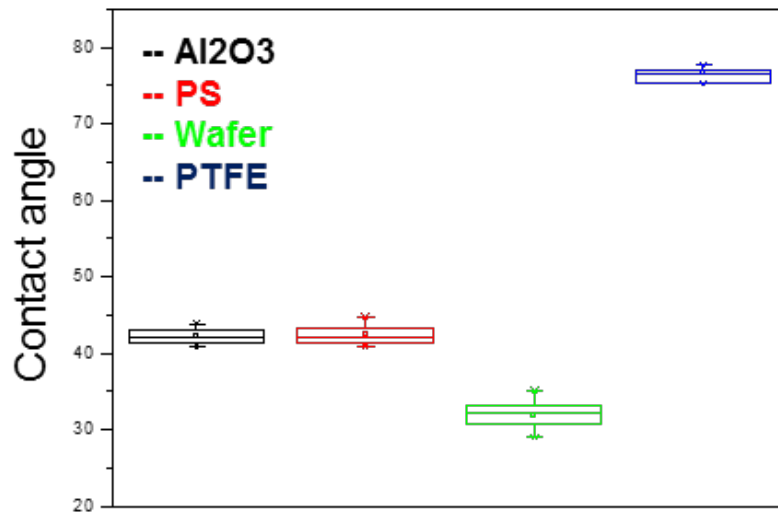


Fig. 34. Contact angle with reference liquids on dimethyl sulfoxide (DMSO)

Fig. 34 shows that the contact angle of dimethyl sulfoxide (DMSO) were displayed on reference materials such as Al₂O₃, Polystyrene (PS), Polytetrafluorethylene (PTFE) and Wafer (Si-111). Because we know the surface free energy of probe solids, we can calculate dimethyl sulfoxide (DMSO). Already we know surface free energy of dimethyl sulfoxide(DMSO)[37], we calculate it again. We get almost similar value about surface free energy. Table 13 shows that the surface free energy of DMSO by using two probe solids such as PTFE and Wafer.

DMSO				
γ_d	γ_P	γ_+	γ_-	γ_{tot}
37.4	6.63	0.762	14.4	44

Table 13. Surface free energy of dimethyl sulfoxide(DMSO) by using 2 probe solids (PTFE, Wafer)

4. Conclusions

When calculating the surface free energy of probe solids such as Al_2O_3 , Polystyrene (PS) and Wafer(Si-111), we can get surface free energy of battery electrolyte. To analyze the surface free energy of PC, we used Al_2O_3 , Polystyrene (PS) and Wafer (Si-111). We confirmed that adequate surface free energy of PC by using 2 probe solids. However, to calculate the more precise surface free energy of battery electrolyte, we need more and adequate probe solids. Also, retain accuracy of contact angle is important because it is sensitive to humidity and temperature.

References

- [1] T. Young, *Philos Trans R Soc London*, 95 (1805) 65-87.
- [2] D.K. Owens, R.C. Wendt, *J Appl Polym Sci*, 13 (1969) 1741-1747.
- [3] W.A. Zisman, *Industrial & Engineering Chemistry*, 55 (1963) 18-38.
- [4] F.M. Fowkes, *Industrial & Engineering Chemistry*, 56 (1964) 40-52.
- [5] C.J. van Oss, M.K. Chaudhury, R.J. Good, *Adv Colloid Interface Sci*, 28 (1987) 35-64.
- [6] B. Jańczuk, W. Wójcik, A. Zdziennicka, *J Colloid Interface Sci*, 157 (1993) 384-393.
- [7] F.M. Fowkes, *The Journal of Adhesion*, 4 (1972) 155-159.
- [8] E. Chibowski, R. Perea-Carpio, *Adv Colloid Interface Sci*, 98 (2002) 245-264.
- [9] H. Dipl.-Phys. Hubert Lechner. Krüss, Germany, in, 1996.
- [10] C.J. Van Oss, R.J. Good, M.K. Chaudhury, *J Colloid Interface Sci*, 111 (1986) 378-390.
- [11] C.J. Van Oss, L. Ju, M.K. Chaudhury, R.J. Good, *J Colloid Interface Sci*, 128 (1989) 313-319.
- [12] M.-S. Wu, T.-L. Liao, Y.-Y. Wang, C.-C. Wan, *J Appl Electrochem*, 34 (2004) 797-805.
- [13] E.W. Washburn, *Physical Review*, 17 (1921) 273-283.
- [14] A. Lundblad, B. Bergman, *J Electrochem Soc*, 144 (1997) 984-987.
- [15] C. Bakli, S. Chakraborty, *Appl Phys Lett*, 101 (2012) 153112.
- [16] L. Dahéron, R. Dedryvère, H. Martinez, D. Flahaut, M. Ménétrier, C. Delmas, D. Gonbeau, *Chem Mater*, 21 (2009) 5607-5616.
- [17] N. Andreu, I. Baraille, H. Martinez, R. Dedryvère, M. Loudet, D. Gonbeau, *J Phys Chem C*, 116 (2012) 20332-20341.
- [18] Y. Zhao, S. Wang, W. Ren, R. Wu, *J Electrochem Soc*, 160 (2013) A82-A86.
- [19] M. S. Whittingham, *Chem. Rev.* 104 (2004) 4271-4302.
- [20] Q. Zhong, A. Bonakdarpour, M. Zhang, Y. Gao, J. R. Dahn, *J. Electrochem. Soc.* 144 (1997) 205– 213.
- [21] Blyr, C. Sigala, G. Amatucci, D. Guyomard, Y. Chabre, J.-M. Tarascon, *J. Electrochem. Soc.* 145 (1998) 194–209.
- [22] A. D. Pasquier, A. B. P. Courjal, D. Larcher, G. Amatucci, B. Gerand, J.-M. Tarascon, *J. Electrochem. Soc.* 146 (1999) 428-436.
- [23] R. Benedek, M. M. Thackeray, *Electrochem. Solid-State. Lett.* 9 (2006) A265-A267.
- [24] J. C. Hunter, *J Solid State Chem.* 39 (1981) 142-147.

- [25] D. H. Jang, Y. J. Shin, S. M. Oh, J. Electrochem. Soc. 143 (1996) 2204-2211.
- [26] Y. Xia, Y. Zhou, M. Yoshio, J. Electrochem. Soc. 144 (1997) 2593-2600.
- [27] S. Komaba, N. Kumagai, Y. Kataoka, Electrochim. Acta 47 (2002) 1229–1239.
- [28] M. Ochida, Y. Domi, T. Doi, S. Tsubouchi, H. Nakagawa, T. Yamanaka, T. Abe, Z. Ogumi, J. Electrochem. Soc. 159 (2012) A961-A966.
- [29] E. Wang, D. Ofer, W. Bowden, N. Iltchev, R. Moses, K. Brandt, J. Electrochem. Soc. 147 (2000) 4023-4028.
- [30] H. Tsunekawa, S. Tanimoto, R. Marubayashi, M. Fujita, K. Kifune, M. Sano, J. Electrochem. Soc. 149 (2002) A1326-A1331.
- [31] O. Levenspiel, *Chemical reaction engineering*, John Wiley & Sons, New York (1972) 357-371.
- [32] A. Blyr, C. Sigala, G. Amatucci, D. Guyomard, Y. Chabre, and J.M. Tarascon, J. Electrochem. Soc. (1998)145, 194.
- [33] Levenspiel, O, *Chemical reaction engineering*, John Wiley & Sons, New York (1999) 3rd edition.
- [34] T. Young, Philos. Trans. Roy. Soc. Lond 95 (1805) 65-87.
- [35] C.S. Stefan, D. Lemordant, B. Claude-Montigny, D. Violleau, J Power Sources, 189 (2009) 1174-1178.
- [36] Sylla, S, Sanchez, J.Y. Armand, M. Electrochim. Acta 37 (1992) 1669.
- [37] van Oss, C. J., Chaudhury, M. K., and Good, R. J., *Separation Sci. Technol.* 24, 15 (1989)

요 약 문

금속 용출에 관한 전해액 구성에 대한 영향과 표면자유에너지와의 관계

리튬이차전지 양극재 중의 LiMn_2O_4 (이하 LMO)는 가격 경쟁력과 환경에 무해하다는 장점으로 활발히 사용되고 있다. 그러나 망간 용출 현상 때문에 셀 수명이 저하되는 단점이 있어 이를 극복하고자 많은 연구들이 진행되어왔다. 하지만 LMO 와 전해액 계면에 관하여 주목하고 그에 대한 kinetics 와 전해액 조성에 관한 영향을 연구하였다. 실험은 LMO 전극을 전해액에 다양한 온도에 대하여 용출시켜 보존하고, 일정 시간이 지난 후 전해액에 용출된 망간을 Atomic absorption spectroscopy (AAS)로 분석하였다. 그 결과, 전해액 조성 중 EC의 함량이 높아질수록 용출 반응 속도 상수 증가하며 망간 용출이 악화되었다. 또한 LMO 전극에서 Mn의 용출은 product layer 를 통한 diffusion 에 의해 발생 하였다. 결국 EC 함량이 높을수록 전극과 전해액 계면에서 용출의 활성화 에너지는 감소하였다.

고용량, 고전압 이차전지의 사용을 위해 삼성분계 양극재인 $\text{LiNi}_{0.6}\text{Co}_{0.2}\text{Mn}_{0.2}\text{O}_2$ 많이 사용이 된다. 보통 용출 현상을 실험하기 위해서는 ICP 혹은 ASS 를 이용하여 측정되는데, 최소 일주일에서 길게는 수주의 시간이 필요하다. 본 연구에서는 삼성분계 양극재의 표면자유에너지를 측정함으로써 단시간에 측정하며 직접적인 용출특성을 예측할 수 있었다. Adsorption 방식으로 접촉각을 측정하여 표면자유에너지를 계산하였다. 금속용출에는 Total, Acid 표면자유에너지가 주도적으로 영향을 미치는 것을 상관관계를 통하여 확인 할 수 있었다.

핵심어: 금속용출, 표면자유에너지, LiMn_2O_4 , $\text{LiNi}_{0.6}\text{Co}_{0.2}\text{Mn}_{0.2}\text{O}_2$, 전해액,

